Direct Relationship between Protein Expression and Progeny Yield of Herpes Simplex Virus 1 Unveils a Rate-limiting Step for Virus Production

Moeka Nobe[1]†, Yuhei Maruzuru[1,2,3]†, Kosuke Takeshima[1,2,3], Fumio Maeda[4], Hideo Kusano[4,5], Raiki Yoshimura[6], Takara Nishiyama[6], Hyeongki Park[6], Yoshitaka Kozaki[6], Shingo Iwami[6], Naoto Koyanagi[1,2,3], Akihisa Kato[1,2,3], Tohru Natsume[4], Shungo Adachi[4,5], and Yasushi Kawaguchi[1,2,3,7]*

[1]Division of Molecular Virology, Department of Microbiology and Immunology, The Institute of Medical Science, The University of Tokyo, Tokyo, Japan

[2]Department of Infectious Disease Control, International Research Center for Infectious Diseases, The Institute of Medical Science, The University of Tokyo, Minato-ku, Tokyo 108-8639, Japan

[3]Research Center for Asian Infectious Diseases, The Institute of Medical Science, The University of Tokyo, Tokyo, Japan

[4]Molecular Profiling Research Center for Drug Discovery (molprof), National Institute of Advanced Industrial Science and Technology (AIST), Tokyo, 135-0064, Japan.

[5]Department of Proteomics, National Cancer Center Research institute, Tokyo, Japan

[6]Interdisciplinary Biology Laboratory (iBLab), Division of Biological Science, Graduate School of Science, Nagoya University, Nagoya 464-8602, Japan

[7]The University of Tokyo, Pandemic Preparedness, Infection and Advanced Research Center, Tokyo, Japan

Short title: A Rate-limiting Step for HSV-1 Production

*Address correspondence to:
Dr. Yasushi Kawaguchi
Division of Molecular Virology
Department of Microbiology and Immunology
The Institute of Medical Science
The University of Tokyo

4-6-1 Shirokanedai, Minato-ku, Tokyo 108-8639, Japan
Phone: 81-3-6409-2070
Fax: 81-3-6409-2072
E-mail: ykawagu@ims.u-tokyo.ac.jp

†These authors contributed equally to this work.

ABSTRACT

Although viral protein expression and progeny virus production were independently shown to be highly heterogenous in individual cells, their direct relationship, analyzed by considering their heterogeneities, has not been investigated to date. This study established a system to fractionate cells infected with a herpesvirus based on the levels of the global expression of viral late proteins, which are largely virion structural proteins, and to titrate virus yields in these fractions. This system demonstrated a direct relationship and indicated there was a threshold for the levels of viral late protein expression for progeny virus production and suggested that viral DNA cleavage/packaging was a rate-limiting step for progeny virus production. These findings, which were masked in previous studies performed at the entire population level, have uncovered a sophisticated viral strategy for efficient progeny virus production and shed new light on an effective target for the development of anti-viral drugs.

51 **INTRODUCTION**

52 The state of viral gene expression has long been thought to be one of the critical
53 determinants for virus progeny production [1]. Viral infection is usually studied at the entire
54 population level by averaging the outcomes of infection from each of large numbers of
55 individual cells. In these previous studies, a relationship between viral gene expression
56 and virus progeny production has necessarily been investigated based on classical time
57 course experiments in which levels of viral gene expression and progeny virus titers were
58 compared at various times after infection. Such studies demonstrated that the levels of
59 viral gene expression, including the expressions of viral mRNA and protein, correlated
60 well with progeny virus yields [2-6]. However, accumulating evidence has indicated that
61 viral infection at the single-cell or subpopulation level is highly heterogeneous, which has
62 been masked in studies performed at the entire population level. Thus, it was reported that
63 the progeny virus yield from individual cells spanned several orders of magnitude [7-14].
64 Classical fluorescence microscopy and recent advances in single-cell RNA-sequencing
65 have enabled the investigation of the state of viral gene expression at the single-cell level,
66 revealing high heterogeneity in individual cells and identifying new subpopulations of
67 infected cells with similar viral gene expression profiles [15-17]. However, there is a lack of
68 information on viral protein expression and virus progeny production in the same

69 individual cell or subpopulation. Therefore, the direct relationship between viral protein
70 expression and progeny virus production, analyzed by considering their heterogeneities
71 at single cell or subpopulation levels, remains to be elucidated. These observations raised
72 a fundamental question as to whether the well-established correlation between viral
73 protein expression and progeny virus production detected at the entire population level
74 by classical time-course experiments [4,6] does reflect a direct relationship between them.

75 Herpes simplex virus 1 (HSV-1), an extensively studied DNA virus, is a
76 ubiquitous human pathogen, causing a variety of diseases including encephalitis, keratitis,
77 and mucocutaneous and skin diseases including herpes labialis, genital herpes and
78 herpetic whitlow [18]. HSV-1 encodes more than 100 different proteins [19-21] and HSV-1
79 genes fall into three major classes: immediate-early (IE), early (E) and late (L), whose
80 expressions are coordinately regulated and sequentially ordered in a cascade during lytic
81 infection [19]. Although there are some exceptions, virion structural proteins are largely
82 encoded by L genes [19]. Replication of the HSV-1 genome and packaging of the replicated
83 viral genomes into nascent capsids occurs in the nucleus [19]. Nascent nucleocapsids are
84 exported to the cytoplasm through the perinuclear space between the inner nuclear
85 membrane and outer nuclear membrane by a nuclear pore-independent and sequential

envelopment/de-envelopment process [19]. In the cytoplasm, capsids acquire a final envelope by budding into cytoplasmic vesicles and become infectious [19].

In this study, we constructed a reporter HSV-1 to monitor the global expression of viral L proteins by analyzing direct and quantitative relationship between L protein expression levels and virus progeny yields by sorting infected cells into subpopulations based on reporter gene expression levels and by determining virus titers in the subpopulations. The clarified relationship indicated a threshold in the levels of HSV-1 L protein expression for progeny virus production, suggesting viral DNA cleavage/packaging is a rate-limiting step for progeny virus production.

96 **RESULTS**

97 **Construction and characterization of a reporter HSV-1 to analyze viral L protein**
98 **expression and virus progeny yields at the subpopulation level.** We constructed a
99 recombinant virus rICP47/vUs11 expressing IE protein ICP47 and L protein Us11 fused
100 to monomeric fluorescent proteins, TagRFP and VenusA206K (TagRFP-ICP47 and
101 Venus-Us11), respectively (Fig. 1A and B). The growth of rICP47/vUs11 was similar to
102 wild-type HSV-1(F) in HeLa cells at a multiplicity of infection (MOI) of 5 and reached a
103 plateau 24 h after infection (Fig. 1C). Flow cytometric analyses showed 92% of HeLa
104 cells inoculated with rICP47/vUs11 at an MOI of 5 were TagRFP positive 24 h after
105 inoculation, indicating that in these experimental settings, most HeLa cells were infected
106 with rICP47/vUs11 and HSV-1 gene expression was initiated in these infected cells (Fig.
107 1D and E). Frequencies of cells positive for Venus and TagRFP, or those positive for
108 TagRFP and negative for Venus, were 67% and 25%, respectively (Fig. 1E). Cells
109 positive for Venus and negative for TagRFP were barely detectable (Fig. 1D and E).
110 Notably, the coefficient of variation (CV) for Venus-Us11 fluorescence intensities in each
111 infected cell was significantly higher than for TagRFP-ICP47 fluorescence (Fig. 1F).

112 To examine whether levels of Venus-Us11 fluorescence in rICP47/vUs11-
113 infected cells were related to those of the global expression of HSV-1 L proteins, HeLa

114 cells infected with rICP47/vUs11 at an MOI of 5 for 24 h were analyzed by flow
115 cytometry and sorted into six subpopulations (f1 to f6) based on the levels of Venus-Us11
116 fluorescence intensities—Venus-Us11 fluorescence intensities increased in
117 subpopulations from f1–f6 (S-Fig. 1A). The subpopulations were then subjected to LC-
118 MS/MS to quantitate peptides of global HSV-1 L proteins (Fig. 2A and S-Fig. 1B).
119 Among the HSV-1 L proteins detected (48 L proteins), there was a strong correlation
120 between the levels of Venus-Us11 fluorescence intensity and the relative abundance of
121 most HSV-1 L proteins including Venus-Us11 (33 L proteins, $r>0.90$, $P<0.001$; 10 L
122 proteins, $r>0.70$, $P<0.01$; 4 L proteins, $r>0.58$, $P<0.05$) but not Us8.5 ($r=0.54$, $P=0.07$).
123 These results suggested that Venus-Us11 fluorescence intensities reflected expression
124 levels of global HSV-1 L proteins in rICP47/vUs11-infected cells.

125 **Specific Venus-Us11 protein expression levels are linked to progeny virus**
126 **production.** To analyze a relationship between expression levels of HSV-1 L proteins
127 and progeny virus yields directly and quantitatively, HeLa cells were infected with
128 rICP47/vUs11 at an MOI of 5, harvested at 4, 6, 8, 10, 12, and 24 h after infection,
129 analyzed by flow cytometry and sorted into entire population (FSC singlet) or six
130 subpopulations (f1 to f6) according to the levels of Venus-Us11 fluorescence intensity

131 (S-Fig. 2). Virus titers in the entire population and each of the subpopulations were
132 determined and virus titers per 10^4 cells were estimated.

133 In agreement with previous reports [4,6], the kinetics of Venus-Us11 fluorescence
134 intensity were similar to those of progeny virus titers (Fig. 3A) and Venus-Us11
135 fluorescence intensities had a high correlation with progeny virus titers at the entire
136 population level (r=0.95) (Fig. 3B). We also calculated virtual titers per 10^4 cells at each
137 timepoint by summating virus titers in subpopulations, obtained by multiplying the
138 estimated virus titer of each subpopulation of 10^4 cells by the ratio of number of cells in
139 the subpopulation to that in the entire population. A viral growth curve based on the
140 virtual titers was almost identical to that based on actual titers in the entire population
141 (Fig. 3C).

142 At the entire population level, virus titers were decreased 6 h after infection due
143 to an eclipse phase of infection and viral replication entered the productive phase between
144 6 and 8 h post-infection (Fig. 3A and C). These results indicated that infectious progeny
145 virus production was detectable 8 h after infection in these experiments. The f4
146 subpopulation emerged at this timepoint (Fig. 3D, F and G, and S-Table 2). Although
147 4.1% of total cells were in the f4 subpopulation 8 h after infection (Fig. 3D, and S-Table
148 2), 55% of progeny infectious virus yields were produced by this subpopulation (Fig. 3E,

149 and S-Table 2). The f5 and f6 subpopulations emerged 10 and 12 h after infection,
150 respectively, when the growth rate had slowed (Fig. 3D, F and G, and S-Table 2). At 10
151 h after infection, 18% of total cells were in the f4 and f5 subpopulations (Fig. 3D, and S-
152 Table 2) and these subpopulations produced 87% of progeny infectious virus yields (Fig.
153 3E, and S-Table 2). At 12 and 24 h post-infection, 33% and 53% of total cells were in the
154 f4 to f6 subpopulations, respectively (Fig. 3D, and S-Table 2), and these subpopulations
155 produced 95% of progeny infectious virus yields (Fig. 3E, and S-Table 2). Similarly, most
156 progeny infectious virus yields were produced by the f4 to f6 subpopulations in HeLa
157 cells using MOIs of 1 and 2.5 at 24 h post-infection and in other cells (Vero, U2Os and
158 HaCaT cells, and human fetal foreskin fibroblasts (HFFF-2)) at MOIs 1 or 2.5 at 12 h
159 post-infection, although the proportion of each subpopulation varied by different MOI
160 and cell type (S-Figs. 3A to D and 4A to D, F to I, K to N and P to S). Notably, the viral
161 growth curve from 8 h post-infection based on the virtual titers using only the data of the
162 f4 to f6 subpopulations was almost identical to that based on the virtual titers using the
163 data of the f1 to f6 populations or actual titers of the entire population (Fig. 4A and B).
164 Similarly, virtual titers using only the data of the f4 to f6 subpopulations in HeLa cells at
165 MOIs of 1 and 2.5 and in Vero, U2OS, and HaCaT cells, and HFFF-2 were also similar
166 to virtual titers using the data of f1 to f6 populations or actual titers in the entire population

167 (S-Figs. 3E to G, 4E, 4J, 4O, and 4T). These results indicated that subpopulations f4 to
168 f6 have a predominant role in yielding progeny infectious viruses, whereas
169 subpopulations f1 to f3 barely produced infectious virions. To obtain evidence to further
170 support this conclusion, we analyzed virion morphogenesis by quantitating the number
171 of virus particles at different morphogenetic stages in HSV-1-infected HeLa cells at an
172 MOI of 5 for 8 (S-Fig. 5) or 24 h (Fig. 5) in each subpopulation f2 to f4 or f5, respectively,
173 by electron microscopy. All virion types were barely detectable in infected cells from
174 subpopulation f2 (Fig. 5 and S-Fig. 5). In subpopulation f3, although nuclear virions were
175 obvious, cytoplasmic virions, and especially enveloped virions in the cytoplasm that were
176 considered infectious, were barely detectable (Fig. 5 and S-Fig. 5). In contrast, enveloped
177 virions were detected in the cytoplasm of 100% of infected cells in the f4 subpopulation
178 at 8 h post-infection (S-Fig. 5) and these virions were detected in the cytoplasm of 70%
179 and 100% of infected cells in the f4 and f5 subpopulations, respectively, at 24 h post-
180 infection (Fig. 5). The proliferative profiles of enveloped virions in the cytoplasm (Fig. 5
181 and S-Fig. 5) were similar to those of infectious virus titers (S-Fig. 6A).

182 We noted that, even at 4 and 6 h post-infection, the virus titers in f1 to f3
183 subpopulations were detectable at a maximum of 2.8×10^2 PFU/10^4 cells (Fig. 3G and S-
184 Table 2). Taken together with the series of observations above (Figs. 3D and E, 4A and

185 B, and 5, and S-Figs. 3, 4, 5, and 6A) indicating that infected cells in subpopulations f1
186 to f3 barely produced infectious virions, it was not likely that infectious virus titers in
187 subpopulations f1 to f3 detected ranging from 2.6×10^1 to 9.3×10^2 PFU/10^4 cells (Fig.
188 3G and S-Table 2) represented progeny virus yields of infected cells in f1 to f3
189 subpopulations. Cells in the f1 to f3 subpopulations were likely to be aborted infected
190 cells and their frequencies 24 h after infection were similar to those reported previously
191 in HeLa cells [13,22].

192 Collectively, these results together with the observation that Venus-Us11
193 fluorescence intensities reflected the expression levels of global HSV-1 L proteins
194 indicated that certain levels of L protein expression were required for progeny virus
195 production and a threshold of progeny virus production existed between Venus-Us11
196 protein expression levels in subpopulations f3 and f4. Notably, Venus-Us11 fluorescence
197 intensities in subpopulations above the threshold (f4 to f6) correlated highly with progeny
198 virus titers (r=0.87) (Fig. 4C). In contrast, a much lower correlation of coefficient (r=0.46)
199 was observed in subpopulations below the threshold (Fig. 4C). Furthermore, virus titers
200 in subpopulations f4 to f6 remained unchanged during HSV-1 infection (Fig. 4D and S-
201 Fig. 6B) indicating L protein expression levels in subpopulations above the threshold
202 were tightly correlated with virus titers independent of the timepoint after infection. Thus,

203 infectious progeny virus production in the entire population over time depended on the
204 proportion of these subpopulations in the entire population.

205 **Virion morphogenesis with a defect in the cleavage/packaging of HSV-1**
206 **DNA genome occurs in the subpopulation below the threshold for progeny virus**
207 **production.** The threshold for progeny virus production detected between Venus-Us11
208 protein expression levels in subpopulations f3 and f4 suggested a rate-limiting viral step
209 for progeny virus production. Conceivably, this defect(s) might be observed in
210 subpopulations below the threshold (f1 to f3) but not in subpopulations above the
211 threshold (f4 to f6). To clarify this rate-limiting viral step, we compared levels of HSV-1
212 DNA genome replication and global viral mRNA expression in subpopulations f1 to f6
213 by quantitative PCR and RNA sequencing, respectively. Amounts of HSV-1 genome
214 DNA increased in the f1 subpopulation and almost reached a plateau between
215 subpopulations f2 and f3 (S-Fig. 7A). Similar proliferative profiles were observed for
216 expressions of each of the 73 HSV-1 mRNAs tested (S-Fig. 7B). Thus, we did not detect
217 any rate-limiting effects of HSV-1 genome replication or viral mRNA expression
218 associated with the threshold for progeny virus production.

219 Next, we visualized virion morphogenesis by electron microscopy focusing on
220 the A, B and C capsids in the nucleus (Fig. 6 and S-Fig. 8). The A and B capsids are

221 incomplete structures resulting from problems in viral DNA genome retention in the
222 capsids and packaging into the capsids, respectively [23-25]. C capsids are mature capsids
223 (nucleocapsids) containing viral DNA genomes reported to be selectively exported to the
224 cytoplasm [26-29]. B capsids accumulated aberrantly in subpopulation f3 and most (90.1%)
225 nuclear capsids in this subpopulation were B capsids (Fig. 6 and S-Fig. 8). The frequency
226 of B capsids in subpopulation f3 was significantly higher than in subpopulations f4 and
227 f5 (Fig. 6B). In contrast, the frequency of C capsids in subpopulation f3 was significantly
228 lower than in subpopulations f4 and f5 (Fig. 6B). In agreement with this and previous
229 reports that C capsids are selectively exported to the cytoplasm [26-29], the frequency of
230 virions in the perinuclear space and cytoplasm in subpopulation f3 was significantly lower
231 than in subpopulations f4 and f5 (Fig. 6C). The frequency of A capsids in subpopulation
232 f3 was comparable to those in subpopulations f4 and f5 (Fig. 6B). The frequencies of each
233 type of nuclear capsid in subpopulations f4 and f5 were similar to those reported
234 previously in wild-type HSV-1-infected HeLa cells [30]. Furthermore, the aberrant
235 accumulation of B capsids and lack of nuclear C capsids and virions in the perinuclear
236 space and cytoplasm in subpopulation f3 were also observed at 8h post-infection (S-Figs.
237 5 and 9). These features of subpopulation f3 were similar to the phenotypes of HSV-
238 mutants with defective viral DNA genome cleavage/packaging including those lacking

239 the portal protein UL6, a terminase subunit (UL15, UL33 or UL28) or a minor capsid
240 protein (UL17 or UL32) [31-37].

241 Collectively, these results suggested that the cleavage/packaging of HSV-1 DNA
242 genome was specifically down-regulated in subpopulations below the threshold and that
243 this viral step was a rate-limiting step for progeny virus production.

244 **A subset of HSV-1 L proteins including components of viral terminase have**
245 **unique protein expression profiles.** We compared global HSV-1 L protein abundance
246 in each subpopulation by LC-MS/MS, and there was a strong correlation between the
247 Venus-Us11 fluorescence intensities and relative abundance of most HSV-1 L proteins
248 detected (Fig. 2B). Therefore, we focused on the abundance profiles of the bottom 10
249 HSV-1 L proteins with a relatively low correlation (Fig. 7A). The abundance profiles of
250 several of these HSV-1 L proteins including UL25, UL3, UL4, UL33, Us10, and UL15
251 (Fig. 7A) differed from those of other HSV-1 L proteins whose abundance continuously
252 increased in subpopulations f1 to f6 (S-Fig. 1B). The abundance of these L proteins in
253 subpopulations f1 to f3 were very low and remained relatively constant, but were
254 increased in subpopulations f4 to f6.

255 Next, to quantitatively evaluate the delayed increase in the abundance of L
256 protein in the subpopulations, a four-parameter logistic regression was used for curve

257 fitting of these profiles 24 h after infection (S-Fig. 10). The x-axis value at which the y-
258 axis value increased by $\log_{10}2$ (2-fold increase in linear scale) from the starting point
259 (x=0) for each curve was defined as the threshold value (TV) (S-Fig. 10 and Fig. 7B). Fig.
260 7C shows the top 10 proteins with the highest TV identified in this analysis. Of particular
261 interest, these included all the subunits of HSV-1 terminase including UL15, UL33, UL28
262 and the HSV-1 portal protein UL6, all of which were reported to be required for viral
263 DNA genome cleavage/packaging[31-34,36]. These results indicated that the expressions of
264 a fraction of L proteins including all the subunits of HSV-1 terminase and the viral portal
265 protein lacked in subpopulations f1 to f3, unlike that of other L proteins, suggesting the
266 expressions of the L proteins are somehow downregulated in subpopulations below the
267 threshold.
268

269 **DISCUSSION**

270 Single-cell analyses have identified new subpopulations of virus-infected cells with
271 similar viral gene expression profiles [15-17]. However, the use of single-cell analyses to
272 investigate both viral gene expression and progeny virus production is limited. Thus,
273 single-cell analyses for both viral RNA synthesis and progeny virus production have been
274 reported for some RNA viruses [10,12,14]; a recent study reported that influenza virus
275 transcription and progeny virus production were poorly correlated at the single cell level
276 [14], and other studies did not focus on the relationship between viral transcription and virus
277 progeny production at the single cell level [10,12]. Furthermore, protein expression and virus
278 progeny production at the single-cell or subpopulation level have not been investigated
279 to date. This study established a system to fractionate HSV-1-infected cells based on
280 global HSV-1 L protein expression levels and to titrate progeny virus yields in these
281 fractions. This established system enabled us to clarify, for the first time, the direct and
282 quantitative relationship between viral protein expression and progeny virus yields, and
283 the clarified relationship indicated a threshold for HSV-1 L protein expression levels for
284 progeny virus production. Such a threshold has not been reported by classical time course
285 studies of most viruses at the entire population level by analyzing the relationship between
286 viral gene expression and progeny virus yield. In contrast, once the levels of HSV-1 L

287 protein expression exceeded the threshold, they were highly correlated with infectious
288 progeny virus yields as reported by our (Fig. 3B) and other previous studies at the entire
289 population level [4,6].

290 The threshold clarified in this study led us to identify the HSV-1 genome DNA
291 cleavage/packaging step was a rate-limiting step for progeny virus production.
292 Supporting this, MS analysis of the global expression of HSV-1 L proteins at the
293 subpopulation level showed the expression of a subset of HSV-1 L proteins including all
294 components of viral terminase and portal protein lacked in subpopulations below the
295 threshold. Conceivably, an anti-viral strategy targeting this bottleneck step for HSV-1
296 production might block progeny virus production effectively. HSV-1 genome DNA
297 cleavage/packaging, which is largely mediated by a specific viral enzyme HSV-1
298 terminase, is essential for viral replication [31,33,34,36], and most targets of antiviral drugs
299 successfully developed to date are viral specific enzymes [38]. Our study at the
300 subpopulation level using this newly established system revealed an ideal target for the
301 development of anti-viral drugs. Notably, the newly established system is simple and
302 widely applicable for studies of the direct relationship between viral gene expression and
303 progeny virus yield of many other DNA and RNA viruses, which might provide specific
304 and conserved insights into mechanisms of progeny virus production in these viruses. It

305 will be particularly interesting to determine whether the rate-limiting step identified in
306 the progeny virus production of HSV-1 is conserved in adenoviruses, which seem to
307 utilize similar DNA genome packaging systems [39].

308 It has long been recognized that much fewer virions are present in the cytoplasm
309 of HSV-1-infected cells compared with the nucleus [40-42]. Our conclusion that the HSV-1
310 genome DNA cleavage/packaging step is a rate-limiting step for progeny virus production
311 is in agreement with these observations as well as earlier reports demonstrating C capsids
312 are selectively exported to the cytoplasm [26-29]. The ate-limiting step identified in this study
313 also suggests a sophisticated strategy of efficient progeny virus production by HSV-1
314 without accumulating progeny nucleocapsids in the cytoplasm, which enables evasion
315 from cytosolic sensors related to innate immune responses. In the cytoplasm, HSV-1
316 nucleocapsids are degraded by proteasomes [43], and viral DNAs are likely to be sensed by
317 cytosolic sensors including cGAS, AIM2, DAI, and RNA polymerase III, which promote
318 innate immune responses [44-49]. Here we showed that, in subpopulation f3, which was
319 likely slightly below the threshold, HSV-1 genome DNA replication had already reached
320 a plateau and B capsid formation was easily observed although C capsid formation was
321 barely detectable. In contrast, in subpopulation f4, which was likely slightly over the
322 threshold, C capsids and all types of virions in the perinuclear space and the cytoplasm

323 were evident. These observations suggested that downregulating the HSV-1 DNA
324 cleavage/packaging might promote the accumulation of nucleocapsid components
325 including capsids and viral genome DNAs in the nucleus as well as other viral proteins
326 required for virion maturation at the NMs and in the cytoplasm at a level sufficient for
327 efficient progeny virus production. Once the viral genome is packaged into a capsid, the
328 following steps for virion maturation might immediately proceed without accumulating
329 any excess nucleocapsids in the cytoplasm, decreasing the chance for HSV-1 to be sensed
330 by innate immune responses in the cytoplasm. IFI16 and hnRNPA2B1 sense HSV-1
331 genome DNA and promote innate immune responses in the nucleus [50-52]. However,
332 replicated HSV-1 genome DNAs and nucleocapsids appear to accumulate in the nucleus
333 of HSV-1-infected cells [19,53,54], suggesting this virus has evolved more effective evasion
334 mechanisms against innate immune responses in the nucleus such that ICP0 counteracts
335 IFI16 [50] and probably, against capsid degradation than those in the cytoplasm.

336 We noted that overall viral mRNA levels increased from the f1 subpopulation
337 and almost reached a plateau between subpopulations f2 and f3 (S-Fig. 4B). In contrast,
338 viral L protein levels continued to increase from the f1 to f6 subpopulations (S-Fig. 1B).
339 Thus, there was a lack of correlation between viral L mRNA levels and viral L protein
340 levels especially in fractions f4 to f6. In agreement with these observations, previous

341 systematic studies quantifying mRNA and protein levels at the genomic scale reported
342 the importance of multiple processes beyond the mRNA concentration that contributed to
343 establishing the level of a protein [55]. These processes include translation rates, translation
344 rate modulation, modulation of a protein's stability, protein synthesis delay, and protein
345 transport [55]. Interestingly, it was reported that HSV-1 VP22 promoted global viral protein
346 expression [56,57], potentially by reducing the dependence of protein synthesis upon cellular
347 ribosomal proteins to support translation during infection [58], and by promoting the
348 translocation of viral L mRNAs to the cytoplasm [59]. HSV-1 might evolve VP22 to
349 promote global viral translation efficiency in specific circumstances such as in
350 subfractions f4 to f6, in which amounts of viral mRNAs are saturated.
351

352 **MATERIALS AND METHODS**

353 **Cells and Viruses.** HeLa, U2OS, HFFF-2, HaCaT, and Vero cells were described
354 previously [20,60]. Wild-type HSV-1(F) was described previously [61].

355 **Generation of a recombinant virus.** Recombinant virus YK410
356 (rICP47/vUs11) in which ICP47 and Us11 were tagged with TagRFP [62] and VenusA206K
357 [63], respectively, were generated by two rounds of two-step Red-mediated mutagenesis
358 using *Escherichia coli* GS1783 containing pYEbac102Cre [61,64], a full-length infectious
359 HSV-1(F) clone, pBS-Venus-KanS [20], pFlag-TagRFP-KanS, and the primers listed in S-
360 Table 1. The viruses used in this study were propagated and titrated in Vero cells.

361 **Plasmids.** pFlag-TagRFP was constructed by amplifying the TagRFP open
362 reading frame (ORF) to introduce a *Kpn*I site without changing the amino acid sequence
363 by PCR from pTagRFP-N1 [65] and cloning it into pFlag-CMV2 (Sigma). pFlag-TagRFP-
364 KanS, used in the two-step Red-mediated mutagenesis procedure, was constructed by
365 amplifying the domain of pEP-KanS [66] carrying the I-*Sce*I site and the kanamycin
366 resistance gene by PCR from pEP-KanS using the primers 5'-
367 GCGGTACCGTGAACAACCACCACTTCAAAGGATGACGACGATAAGTAGGG-
368 3' and 5'-
369 GCGGTACCCTCCATGTACAGCTTCATGTCAACCAATTAACCAATTCTGATTA

370 G-3' and cloning it into the *Kpn*I site of pFlag-TagRFP. pGEX-ICP47 was constructed
371 by amplifying the ICP47 ORF by PCR from the HSV-1(F) genome and cloning it into
372 pGEX-4T-1.

373 **Antibodies.** Commercial antibodies used in this study included mouse
374 monoclonal antibody to α-tubulin (DM1A; Sigma), and rabbit monoclonal antibodies to
375 GFP (598; MBL) and TagRFP (AB233; Evrogen). Rabbit polyclonal antibodies to US11
376 were described previously [41]. To generate a rabbit polyclonal antibody to ICP47, a rabbit
377 was immunized, according to the standard protocol at MBL, with GST-ICP47 expressed
378 in *E. coli* and purified as described previously [20]. Serum from the immunized rabbit was
379 used as the anti-ICP47 polyclonal antibody.

380 **Immunoblotting.** Immunoblotting was performed as described previously [67].

381 **Flow cytometry.** HeLa cells infected with HSV-1(F) or YK410 (rICP47/vUs11)
382 were washed with phosphate buffered saline (PBS) and detached with 0.25%
383 trypsin/EDTA solution (Wako). Then, the cells were suspended in PBS containing 2%
384 FCS, filtered through a 35-μm pore-cell strainer (#352235, Corning) and subjected to
385 FACS analysis with BD FACS Melody (Becton Dickinson). The data were analyzed with
386 BD FACSChorus (Becton Dickinson) software or FlowJo 10.8.1 software (Becton
387 Dickinson).

388 **Determination of viral titer in cells fractionated by cell sorting.** HeLa cells
389 were infected with YK410 (rICP47/vUs11) at an MOI of 5. At the indicated times after
390 infection, cells were detached and suspended as described above. Then, 1.5×10^4 to $3 \times$
391 10^4 cells in the f1 to f6 subpopulations, and the entire cell population (FSC-singlet), were
392 sorted into medium 199 containing 1% FCS by FACS Melody (Becton Dickinson). The
393 sorted cells were freeze-thawed once, sonicated, and virus titers were determined by
394 plaque assay using Vero cells. The average virus titer per single cell was obtained by
395 dividing the obtained virus titer by the number of sorted cells. Data are presented as the
396 PFU per 10^4 cells.

397 **Calculation of the proportion of virus titers in each subpopulation and the**
398 **virtual titer.** PFU_{fi}, which represents the viral titer of each subpopulation fi (i = 1 to 6),
399 was obtained using the following equation:

400 $PFU_{fi} = PFU_{fi/cell} \times 10^4 \times PR_{Fi} / 100$

401 where $PFU_{fi/cell}$ is the average viral titer per single cell belonging to the fi subpopulation
402 (from Fig. 3F and G) and PR_{fi} is the proportion (%) of cells in the fi fraction in the entire
403 population (from Fig. 3D). The virtual titer (VT), which represents the sum of PFU_{fi} was
404 obtained as follows:

405 $VT = PFU_{f1} + PFU_{f2} + PFU_{f3} + PFU_{f4} + PFU_{f5} + PFU_{f6}$

406 % of PFU_{Pi}, which represents the proportion of viral titers in the fi subpopulation
407 accounted for in the entire population (Fig. 3E) was obtained using the following
408 equation:
409 % of $PFU_{fi} = PFU_{fi} / VT \times 100$
410 **LC-MS/MS analysis of cells fractionated by cell sorting.** HeLa cells were
411 infected with rICP47/vUs11 at an MOI of 5 for 24 h. Then, cells were detached and
412 suspended as described above. Next, 10^5 cells in the f1 to f6 subpopulation were sorted
413 into PBS by BD FACS Melody (Becton Dickinson), pelleted by centrifugation, and lysed
414 with lysis buffer (0.1 M of Tris-HCl (pH 8.0), 1% SDS). To remove SDS from samples,
415 we used the methanol-chloroform protein precipitation method. Briefly, we added 4
416 volumes of methanol, 1 volume of chloroform, and 3 volumes of water to the eluted
417 sample and mixed thoroughly. The samples were centrifuged at 15,000 rpm for 10 min,
418 the water phase was carefully removed, and then 4 volumes of methanol were added to
419 the samples. The samples were centrifuged at 15,000 rpm for 10 min, and the supernatant
420 was removed. The pellet was washed once with 100% ice-cold acetone. The precipitated
421 protein was re-dissolved in guanidine hydrochloride, reduced with TCEP, alkylated with
422 iodoacetamide, and digested with lysyl endopeptidase and trypsin. The resulting digested
423 peptides were analyzed using an Evosep One LC system (EVOSEP) connected to a Q-

424 Exactive HF-X mass spectrometer (Thermo) with a Dream spray tip (AMR) and a 15 cm
425 × 150 μm column packed with 1.9-μm C18-beads (Evosep). The mobile phases were
426 comprised of 0.1% FA as solution A and 0.1% FA/99.9% ACN as solution B. The
427 analysis was performed in the data-dependent acquisition mode, where the top 25
428 recorded mass spectrometry spectra between 380 and 1500 m/z were selected. Survey
429 scans were acquired at a resolution of 60,000 at m/z 200, and the tandem mass
430 spectrometry (MS/MS) resolution was set to 15,000 at m/z 200. All MS/MS spectra were
431 searched against the protein sequences of the HSV protein database and human Swiss-
432 Prot database using Proteome Discoverer 2.2 (Thermo) with the SEQUEST search engine,
433 and the result of HSV proteins was extracted. The false discovery rate (FDR) was set to
434 1% on peptide spectrum match (PSM).

435 **Data processing of LC-MS/MS data.** Normalization was performed on
436 quantitative values using the method built into the Discoverer 2.2 software. Briefly, the
437 Total Peptide Amount mode was used to normalize between samples, and the On All
438 Average mode was used to normalize between identified proteins. The subsequent
439 analysis was performed using only the extracted data for HSV proteins. The
440 normalization method in each mode was as follows. The Total Peptide Amount mode
441 sums the peptide group abundances for each sample and determines the maximum sum

442 for all files. The normalization factor is the factor of the sum of the samples and the
443 maximum sum in all files. The On All Average mode aggregates all the abundance or
444 normalized abundance values per sample and scales the abundance values of each sample
445 so that the average of all samples is 100. When a peptide was not detected in four technical
446 replicates from one sample of each subpopulation, the protein was considered
447 undetectable in that subpopulation. When a peptide was not detected in a replicate of each
448 subpopulation, the missing value was complemented with the mean value of abundances
449 in technical replicates where the peptide was detected. The mean value of abundances
450 from four technical replicates were used as the value of a single experiment. The relative
451 abundance of each HSV-1 L protein was calculated relative to the subpopulation with the
452 lowest mean abundance for two biologically independent experiments as 1.

453 **RNA-sequencing in cells fractionated by cell sorting.** HeLa cells were
454 infected with YK410 (rICP47/vUs11) at an MOI of 5 for 24 h. Then, cells were detached
455 and suspended as described above. Next, 5×10^5 cells in the f1 to f6 subpopulations were
456 sorted into PBS by BD FACS Melody (Becton Dickinson). After centrifugation, total
457 RNA from fractionated cells was isolated with a High Pure RNA Isolation kit (Roche).
458 (i) Each cDNA was generated using a Clontech SMART-Seq HT Kit (Takara Clontech,
459 Mountain View, CA, USA), and each library was prepared using a Nextera XT DNA

460 Library Prep Kit (Illumina, San Diego, USA). Sequencing was performed on the
461 DNBSEQ-G400 platform in the 100+100-base paired-end mode. (ii) Generated reads
462 were a mixture of human reads and HSV-1 reads. For human data, generated reads were
463 mapped to the human (hg19) reference genome using TopHat v2.1.1 combined with
464 Bowtie2 ver. 2.2.8 and SAMtools ver. 0.1.18. For HSV-1, generated reads were mapped
465 to the HSV-1 (GenBank: GU734771.1) reference genome using HISAT2 v2.1.0. (iii) The
466 quantification to obtain the read counts of each gene from HSV-1 was performed using
467 featureCounts of subread-2.0.0 with option -M --fraction. With the length data of each
468 gene (another output of the featureCounts), fragments per kilobase of exon per million
469 mapped fragments (FPKMs) were calculated according to the definition. The FPKM of
470 HSV-1 genes was multiplied by (total number of mapped reads of the HSV-1
471 genome)/{(total number of mapped reads of the human genome) + (total number of
472 mapped reads of the HSV-1 genome)}, normalized by the amount relative to the value of
473 the f1 fraction.

474 **Quantification of HSV-1 DNA in cells fractionated by cell sorting.** HeLa cells
475 were infected with YK410 (rICP47/vUs11) at an MOI of 5 for 24 h. Then, cells were
476 detached and suspended as described above. Next, 5×10^4 cells in the f1 to f6
477 subpopulations were sorted into PBS by BD FACS Melody (Becton Dickinson). After

478 centrifugation, total DNA from fractionated cells was isolated with NucleoSpin Tissue
479 XS (TAKARA) according to the manufacturer's instructions. The amount of HSV-1
480 DNA was quantified using the Universal Probe Library (Roche) with TaqMan Master
481 (Roche) and the LightCycler 96 System (Roche) according to the manufacturer's
482 instructions. Primers and probes were designed using probe finder software within the
483 region encoding ICP27 in the HSV-1 genome, and within the region encoding 18S rRNA
484 in the human genome. The primer and probe sequences for ICP27 (for HSV-1 DNA) were
485 5′-TCCGACAGCGATCTGGAC-3′, 5′-TCCGACGAGGAACACTCC-3′, and Universal
486 ProbeLibrary probe 56, and for 18S rRNA (for human DNA) the sequences were 5′-
487 GCAATTATTCCCCATGAACG-3′, 5′-GGGACTTAATCAACGCAAGC-3′, and
488 Universal ProbeLibrary probe 48. The ΔCt was calculated by subtracting the Ct value of
489 HSV-1 DNA by the Ct value of human DNA. The relative amount of HSV-1 DNA to
490 human DNA ($2^{-\Delta Ct}$) was normalized relative to the value of the f1 subpopulation.

491 **Electron microscopic analysis of cells fractionated by cell sorting.** HeLa cells
492 were infected with YK410 (rICP47/vUs11) at an MOI of 5 for 8 h or 24 h. Then, cells
493 were detached and suspended as described above. Next, 5×10^5 to 1×10^6 cells in the f2
494 to f4 (8 h) or f2 to f5 (24 h) subpopulations were sorted by BD FACS Melody (Becton
495 Dickinson). After centrifugation, the pelleted cells were examined by ultrathin-section

496 electron microscopy as described previously [68] except using JEM-1400 Flash microscope
497 (JEOL).

498 **Statistical analysis.** The unpaired Student's *t*-test was used to compare two
499 groups. One-way ANOVA followed by the Tukey multiple comparisons test, or Mann-
500 Whitney *U*-test followed by Bonferroni correction were used for multiple comparisons.
501 A P-value < 0.05 was considered statistically significant. For the statistical comparison
502 of viral titers, data were converted to common logarithms ($\log_{10}$). Pearson correlation
503 coefficients (r) and p-values were calculated on $\log_{10}$ transformed data. GraphPad Prism
504 10 (GraphPad Software) was used to perform statistical analyses.

505 **Classification of HSV-1 genes.** HSV-1 genes were classified into IE, E, and L
506 genes as described previously [19].

507 **Curve fitting.** To describe the abundance profiles of HSV-1 L proteins, we
508 mainly used the following mathematical model developed by dose response modeling [69].

509 $$f(x) = c + \frac{d - c}{1 + \exp\big(b(x - a)\big)} \qquad (1)$$

510 The variable $f(x)$ is the abundance profiles of HSV-1 L proteins. The parameter a is
511 the inflection point of the curve for this model, that is, the point where a change in
512 acceleration in the curve occurs. The parameter b is a slope parameter and the

parameters c and d are the lower and upper horizontal asymptotes or limits, respectively.

Fitting was performed by drc package in R, which estimates the parameters with nonlinear least squares under the assumption of normally distributed response values [70].

518 **REFERENCES**

519 1. Whelan, S. (2013). Viral Replication Strategies. In Fields virology, D.M. Knipe, P.M.
520 Howley, J.I. Cohen, D.E. Griffin, R.A. Lamb, M.A. Martin, V.R. Racaniello, and B.
521 Roizman, eds. (Lippincott-Williams & Wilkins), pp. 105-126.
522 2. Brown, D.M., Kauder, S.E., Cornell, C.T., Jang, G.M., Racaniello, V.R., and Semler,
523 B.L. (2004). Cell-dependent role for the poliovirus 3' noncoding region in positive-
524 strand RNA synthesis. J Virol *78*, 1344-1351. 10.1128/jvi.78.3.1344-1351.2004.
525 3. Kim, D., Kim, S., Park, J., Chang, H.R., Chang, J., Ahn, J., Park, H., Park, J., Son,
526 N., Kang, G., et al. (2021). A high-resolution temporal atlas of the SARS-CoV-2
527 translatome and transcriptome. Nat Commun *12*, 5120. 10.1038/s41467-021-25361-
528 5.
529 4. Lloyd, M.G., Yee, M.B., Flot, J.S., Liu, D., Geiler, B.W., Kinchington, P.R., and Moffat,
530 J.F. (2022). Development of Robust Varicella Zoster Virus Luciferase Reporter
531 Viruses for In Vivo Monitoring of Virus Growth and Its Antiviral Inhibition in
532 Culture, Skin, and Humanized Mice. Viruses *14*. 10.3390/v14040826.
533 5. Ouwendijk, W.J.D., Dekker, L.J.M., van den Ham, H.J., Lenac Rovis, T., Haefner,
534 E.S., Jonjic, S., Haas, J., Luider, T.M., and Verjans, G. (2020). Analysis of Virus and
535 Host Proteomes During Productive HSV-1 and VZV Infection in Human Epithelial
536 Cells. Front Microbiol *11*, 1179. 10.3389/fmicb.2020.01179.
537 6. Tamura, T., Fukuhara, T., Uchida, T., Ono, C., Mori, H., Sato, A., Fauzyah, Y.,
538 Okamoto, T., Kurosu, T., Setoh, Y.X., et al. (2018). Characterization of Recombinant

539 Flaviviridae Viruses Possessing a Small Reporter Tag. J Virol *92*. 10.1128/JVI.01582-
540 17.
541 7. Delbruck, M. (1945). The burst size distribution in the growth of bacterial viruses
542 (bacteriophages). J Bacteriol *50*, 131-135. 10.1128/JB.50.2.131-135.1945.
543 8. Zhu, Y., Yongky, A., and Yin, J. (2009). Growth of an RNA virus in single cells reveals
544 a broad fitness distribution. Virology *385*, 39-46. 10.1016/j.virol.2008.10.031.
545 9. Timm, A., and Yin, J. (2012). Kinetics of virus production from single cells. Virology
546 *424*, 11-17. 10.1016/j.virol.2011.12.005.
547 10. Schulte, M.B., and Andino, R. (2014). Single-cell analysis uncovers extensive
548 biological noise in poliovirus replication. J Virol *88*, 6205-6212. 10.1128/JVI.03539-
549 13.
550 11. Combe, M., Garijo, R., Geller, R., Cuevas, J.M., and Sanjuan, R. (2015). Single-Cell
551 Analysis of RNA Virus Infection Identifies Multiple Genetically Diverse Viral
552 Genomes within Single Infectious Units. Cell Host Microbe *18*, 424-432.
553 10.1016/j.chom.2015.09.009.
554 12. Heldt, F.S., Kupke, S.Y., Dorl, S., Reichl, U., and Frensing, T. (2015). Single-cell
555 analysis and stochastic modelling unveil large cell-to-cell variability in influenza A
556 virus infection. Nat Commun *6*, 8938. 10.1038/ncomms9938.
557 13. Wildy, P., Stoker, M.G.P., and Ross, R.W. (1959). Release of Herpes Virus from
558 Solitary HeLa Cells. Journal of General Microbiology *20*, 105-112. 10.1099/00221287-
559 20-1-105.

560 14. Bacsik, D.J., Dadonaite, B., Butler, A., Greaney, A.J., Heaton, N.S., and Bloom, J.D.
561 (2023). Influenza virus transcription and progeny production are poorly correlated in
562 single cells. Elife *12*. 10.7554/eLife.86852.
563 15. Drayman, N., Patel, P., Vistain, L., and Tay, S. (2019). HSV-1 single-cell analysis
564 reveals the activation of anti-viral and developmental programs in distinct sub-
565 populations. Elife *8*. 10.7554/eLife.46339.
566 16. Ku, C., Sheyn, U., Sebe-Pedros, A., Ben-Dor, S., Schatz, D., Tanay, A., Rosenwasser,
567 S., and Vardi, A. (2020). A single-cell view on alga-virus interactions reveals
568 sequential transcriptional programs and infection states. Sci Adv *6*, eaba4137.
569 10.1126/sciadv.aba4137.
570 17. Suomalainen, M., and Greber, U.F. (2021). Virus Infection Variability by Single-Cell
571 Profiling. Viruses *13*. 10.3390/v13081568.
572 18. Knipe, D.M., Heldwein, E.E., Mohr, I.J., Sodroski, C.N., Whitley, R.J., and Johnston,
573 C. (2022). Herpes Simplex Viruses: Pathogenesis and Clinical Insights. In Fields
574 virology, P.M. Howley, D.M. Knipe, B. Damania, J.I. Cohen, S.P.J. Whelan, E.O.
575 Freed, and L. Enquist, eds. (Lippincott-Williams & Wilkins), pp. 297-323.
576 19. Roizman, B., Knipe, D.M., and Whitley, R.J. (2013). Herpes simplex viruses. In Fields
577 virology, D.M. Knipe, P.M. Howley, J.I. Cohen, D.E. Griffin, R.A. Lamb, M.A. Martin,
578 V.R. Racaniello, and B. Roizman, eds. (Lippincott-Williams & Wilkins), pp. 1823-
579 1897.
580 20. Kato, A., Adachi, S., Kawano, S., Takeshima, K., Watanabe, M., Kitazume, S., Sato,
581 R., Kusano, H., Koyanagi, N., Maruzuru, Y., et al. (2020). Identification of a herpes

582 simplex virus 1 gene encoding neurovirulence factor by chemical proteomics. Nat
583 Commun *11*, 4894. 10.1038/s41467-020-18718-9.
584 21. Whisnant, A.W., Jurges, C.S., Hennig, T., Wyler, E., Prusty, B., Rutkowski, A.J.,
585 L'Hernault, A., Djakovic, L., Gobel, M., Doring, K., et al. (2020). Integrative
586 functional genomics decodes herpes simplex virus 1. Nat Commun *11*, 2038.
587 10.1038/s41467-020-15992-5.
588 22. Cohen, E.M., Avital, N., Shamay, M., and Kobiler, O. (2020). Abortive herpes simplex
589 virus infection of nonneuronal cells results in quiescent viral genomes that can
590 reactivate. Proc Natl Acad Sci U S A *117*, 635-640. 10.1073/pnas.1910537117.
591 23. Cardone, G., Heymann, J.B., Cheng, N., Trus, B.L., and Steven, A.C. (2012).
592 Procapsid assembly, maturation, nuclear exit: dynamic steps in the production of
593 infectious herpesvirions. Adv Exp Med Biol *726*, 423-439. 10.1007/978-1-4614-0980-
594 9_19.
595 24. Homa, F.L. (1997). Capsid assembly and DNA packaging in herpes simplex virus.
596 Reviews in medical virology *7*, 107-122.
597 25. Baines, J.D. (2011). Herpes simplex virus capsid assembly and DNA packaging: a
598 present and future antiviral drug target. Trends Microbiol *19*, 606-613.
599 10.1016/j.tim.2011.09.001.
600 26. Takeshima, K., Arii, J., Maruzuru, Y., Koyanagi, N., Kato, A., and Kawaguchi, Y.
601 (2019). Identification of the Capsid Binding Site in the Herpes Simplex Virus 1
602 Nuclear Egress Complex and Its Role in Viral Primary Envelopment and Replication.
603 J Virol *93*. 10.1128/JVI.01290-19.

604 27. Yang, K., and Baines, J.D. (2011). Selection of HSV capsids for envelopment involves
605 interaction between capsid surface components pUL31, pUL17, and pUL25. Proc
606 Natl Acad Sci U S A *108*, 14276-14281. 10.1073/pnas.1108564108.
607 28. Yang, K., Wills, E., Lim, H.Y., Zhou, Z.H., and Baines, J.D. (2014). Association of
608 herpes simplex virus pUL31 with capsid vertices and components of the capsid
609 vertex-specific complex. J Virol *88*, 3815-3825. 10.1128/JVI.03175-13.
610 29. Johnson, D.C., and Baines, J.D. (2011). Herpesviruses remodel host membranes for
611 virus egress. Nat Rev Microbiol *9*, 382-394. 10.1038/nrmicro2559.
612 30. Khadivjam, B., Bonneil, E., Thibault, P., and Lippe, R. (2023). RNA helicase DDX3X
613 modulates herpes simplex virus 1 nuclear egress. Commun Biol *6*, 134.
614 10.1038/s42003-023-04522-w.
615 31. Heming, J.D., Conway, J.F., and Homa, F.L. (2017). Herpesvirus Capsid Assembly
616 and DNA Packaging. Adv Anat Embryol Cell Biol *223*, 119-142. 10.1007/978-3-319-
617 53168-7_6.
618 32. Patel, A.H., Rixon, F.J., Cunningham, C., and Davison, A.J. (1996). Isolation and
619 characterization of herpes simplex virus type 1 mutants defective in the UL6 gene.
620 Virology *217*, 111-123. 10.1006/viro.1996.0098.
621 33. Baines, J.D., Cunningham, C., Nalwanga, D., and Davison, A. (1997). The U(L)15
622 gene of herpes simplex virus type 1 contains within its second exon a novel open
623 reading frame that is translated in frame with the U(L)15 gene product. J Virol *71*,
624 2666-2673. 10.1128/JVI.71.4.2666-2673.1997.

625 34. Yang, K., Dang, X., and Baines, J.D. (2017). A Domain of Herpes Simplex Virus
626 pU(L)33 Required To Release Monomeric Viral Genomes from Cleaved Concatemeric
627 DNA. J Virol *91*. 10.1128/JVI.00854-17.
628 35. Salmon, B., Cunningham, C., Davison, A.J., Harris, W.J., and Baines, J.D. (1998).
629 The herpes simplex virus type 1 U(L)17 gene encodes virion tegument proteins that
630 are required for cleavage and packaging of viral DNA. J Virol *72*, 3779-3788.
631 10.1128/JVI.72.5.3779-3788.1998.
632 36. Tengelsen, L.A., Pederson, N.E., Shaver, P.R., Wathen, M.W., and Homa, F.L. (1993).
633 Herpes simplex virus type 1 DNA cleavage and encapsidation require the product of
634 the UL28 gene: isolation and characterization of two UL28 deletion mutants. J Virol
635 *67*, 3470-3480. 10.1128/JVI.67.6.3470-3480.1993.
636 37. Lamberti, C., and Weller, S.K. (1998). The herpes simplex virus type 1
637 cleavage/packaging protein, UL32, is involved in efficient localization of capsids to
638 replication compartments. J Virol *72*, 2463-2473. 10.1128/JVI.72.3.2463-2473.1998.
639 38. Tompa, D.R., Immanuel, A., Srikanth, S., and Kadhirvel, S. (2021). Trends and
640 strategies to combat viral infections: A review on FDA approved antiviral drugs. Int
641 J Biol Macromol *172*, 524-541. 10.1016/j.ijbiomac.2021.01.076.
642 39. Ahi, Y.S., and Mittal, S.K. (2016). Components of Adenovirus Genome Packaging.
643 Front Microbiol *7*, 1503. 10.3389/fmicb.2016.01503.
644 40. Lymberopoulos, M.H., Bourget, A., Ben Abdeljelil, N., and Pearson, A. (2011).
645 Involvement of the UL24 protein in herpes simplex virus 1-induced dispersal of B23
646 and in nuclear egress. Virology *412*, 341-348. 10.1016/j.virol.2011.01.016.

647 41. Takeshima, K., Maruzuru, Y., Koyanagi, N., Kato, A., and Kawaguchi, Y. (2022).
648 Redundant and Specific Roles of A-Type Lamins and Lamin B Receptor in Herpes
649 Simplex Virus 1 Infection. J Virol *96*, e0142922. 10.1128/jvi.01429-22.
650 42. Hutchinson, L., and Johnson, D.C. (1995). Herpes simplex virus glycoprotein K
651 promotes egress of virus particles. J Virol *69*, 5401-5413. 10.1128/JVI.69.9.5401-
652 5413.1995.
653 43. Horan, K.A., Hansen, K., Jakobsen, M.R., Holm, C.K., Soby, S., Unterholzner, L.,
654 Thompson, M., West, J.A., Iversen, M.B., Rasmussen, S.B., et al. (2013). Proteasomal
655 degradation of herpes simplex virus capsids in macrophages releases DNA to the
656 cytosol for recognition by DNA sensors. J Immunol *190*, 2311-2319.
657 10.4049/jimmunol.1202749.
658 44. Chiu, Y.H., Macmillan, J.B., and Chen, Z.J. (2009). RNA polymerase III detects
659 cytosolic DNA and induces type I interferons through the RIG-I pathway. Cell *138*,
660 576-591. 10.1016/j.cell.2009.06.015.
661 45. Takaoka, A., Wang, Z., Choi, M.K., Yanai, H., Negishi, H., Ban, T., Lu, Y., Miyagishi,
662 M., Kodama, T., Honda, K., et al. (2007). DAI (DLM-1/ZBP1) is a cytosolic DNA sensor
663 and an activator of innate immune response. Nature *448*, 501-505.
664 10.1038/nature06013.
665 46. Sun, L., Wu, J., Du, F., Chen, X., and Chen, Z.J. (2013). Cyclic GMP-AMP synthase
666 is a cytosolic DNA sensor that activates the type I interferon pathway. Science *339*,
667 786-791. 10.1126/science.1232458.

668 47. Li, X.D., Wu, J., Gao, D., Wang, H., Sun, L., and Chen, Z.J. (2013). Pivotal roles of
669 cGAS-cGAMP signaling in antiviral defense and immune adjuvant effects. Science
670 *341*, 1390-1394. 10.1126/science.1244040.
671 48. Maruzuru, Y., Ichinohe, T., Sato, R., Miyake, K., Okano, T., Suzuki, T., Koshiba, T.,
672 Koyanagi, N., Tsuda, S., Watanabe, M., et al. (2018). Herpes Simplex Virus 1 VP22
673 Inhibits AIM2-Dependent Inflammasome Activation to Enable Efficient Viral
674 Replication. Cell Host Microbe *23*, 254-265 e257. 10.1016/j.chom.2017.12.014.
675 49. Lee, S., Karki, R., Wang, Y., Nguyen, L.N., Kalathur, R.C., and Kanneganti, T.D.
676 (2021). AIM2 forms a complex with pyrin and ZBP1 to drive PANoptosis and host
677 defence. Nature *597*, 415-419. 10.1038/s41586-021-03875-8.
678 50. Orzalli, M.H., DeLuca, N.A., and Knipe, D.M. (2012). Nuclear IFI16 induction of IRF-
679 3 signaling during herpesviral infection and degradation of IFI16 by the viral ICP0
680 protein. Proc Natl Acad Sci U S A *109*, E3008-3017. 10.1073/pnas.1211302109.
681 51. Li, T., Diner, B.A., Chen, J., and Cristea, I.M. (2012). Acetylation modulates cellular
682 distribution and DNA sensing ability of interferon-inducible protein IFI16. Proc Natl
683 Acad Sci U S A *109*, 10558-10563. 10.1073/pnas.1203447109.
684 52. Wang, L., Wen, M., and Cao, X. (2019). Nuclear hnRNPA2B1 initiates and amplifies
685 the innate immune response to DNA viruses. Science *365*. 10.1126/science.aav0758.
686 53. Morgan, C., Ellison, S.A., Rose, H.M., and Moore, D.H. (1954). Structure and
687 development of viruses as observed in the electron microscope. I. Herpes simplex
688 virus. J Exp Med *100*, 195-202. 10.1084/jem.100.2.195.

689 54. de Bruyn Kops, A., and Knipe, D.M. (1988). Formation of DNA replication structures
690 in herpes virus-infected cells requires a viral DNA binding protein. Cell *55*, 857-868.
691 10.1016/0092-8674(88)90141-9.
692 55. Liu, Y., Beyer, A., and Aebersold, R. (2016). On the Dependency of Cellular Protein
693 Levels on mRNA Abundance. Cell *165*, 535-550. 10.1016/j.cell.2016.03.014.
694 56. Duffy, C., Mbong, E.F., and Baines, J.D. (2009). VP22 of herpes simplex virus 1
695 promotes protein synthesis at late times in infection and accumulation of a subset of
696 viral mRNAs at early times in infection. J Virol *83*, 1009-1017. 10.1128/JVI.02245-
697 07.
698 57. Tanaka, M., Kato, A., Satoh, Y., Ide, T., Sagou, K., Kimura, K., Hasegawa, H., and
699 Kawaguchi, Y. (2012). Herpes simplex virus 1 VP22 regulates translocation of
700 multiple viral and cellular proteins and promotes neurovirulence. J Virol *86*, 5264-
701 5277. 10.1128/JVI.06913-11.
702 58. Vink, E.I., Andrews, J., Duffy, C., and Mohr, I. (2021). Preventing translational
703 inhibition from ribosomal protein insufficiency by a herpes simplex virus-encoded
704 ribosome-associated protein. Proc Natl Acad Sci U S A *118*. 10.1073/pnas.2025546118.
705 59. Pheasant, K., Moller-Levet, C.S., Jones, J., Depledge, D., Breuer, J., and Elliott, G.
706 (2018). Nuclear-cytoplasmic compartmentalization of the herpes simplex virus 1
707 infected cell transcriptome is co-ordinated by the viral endoribonuclease vhs and
708 cofactors to facilitate the translation of late proteins. PLoS Pathog *14*, e1007331.
709 10.1371/journal.ppat.1007331.

710 60. Sato, Y., Kato, A., Maruzuru, Y., Oyama, M., Kozuka-Hata, H., Arii, J., and
711 Kawaguchi, Y. (2016). Cellular Transcriptional Coactivator RanBP10 and Herpes
712 Simplex Virus 1 ICP0 Interact and Synergistically Promote Viral Gene Expression
713 and Replication. J Virol *90*, 3173-3186. 10.1128/JVI.03043-15.
714 61. Tanaka, M., Kagawa, H., Yamanashi, Y., Sata, T., and Kawaguchi, Y. (2003).
715 Construction of an excisable bacterial artificial chromosome containing a full-length
716 infectious clone of herpes simplex virus type 1: viruses reconstituted from the clone
717 exhibit wild-type properties in vitro and in vivo. J Virol *77*, 1382-1391.
718 10.1128/jvi.77.2.1382-1391.2003.
719 62. Merzlyak, E.M., Goedhart, J., Shcherbo, D., Bulina, M.E., Shcheglov, A.S., Fradkov,
720 A.F., Gaintzeva, A., Lukyanov, K.A., Lukyanov, S., Gadella, T.W., and Chudakov,
721 D.M. (2007). Bright monomeric red fluorescent protein with an extended fluorescence
722 lifetime. Nat Methods *4*, 555-557. 10.1038/nmeth1062.
723 63. Kremers, G.J., Goedhart, J., van Munster, E.B., and Gadella, T.W., Jr. (2006). Cyan
724 and yellow super fluorescent proteins with improved brightness, protein folding, and
725 FRET Forster radius. Biochemistry *45*, 6570-6580. 10.1021/bi0516273.
726 64. Kato, A., Oda, S., Watanabe, M., Oyama, M., Kozuka-Hata, H., Koyanagi, N.,
727 Maruzuru, Y., Arii, J., and Kawaguchi, Y. (2018). Roles of the Phosphorylation of
728 Herpes Simplex Virus 1 UL51 at a Specific Site in Viral Replication and
729 Pathogenicity. J Virol *92*. 10.1128/JVI.01035-18.
730 65. Arii, J., Takeshima, K., Maruzuru, Y., Koyanagi, N., Nakayama, Y., Kato, A., Mori,
731 Y., and Kawaguchi, Y. (2022). Role of the Arginine Cluster in the Disordered Domain

732 of Herpes Simplex Virus 1 UL34 for the Recruitment of ESCRT-III for Viral Primary
733 Envelopment. J Virol *96*, e0170421. 10.1128/JVI.01704-21.
734 66. Tischer, B.K., von Einem, J., Kaufer, B., and Osterrieder, N. (2006). Two-step red-
735 mediated recombination for versatile high-efficiency markerless DNA manipulation
736 in Escherichia coli. Biotechniques *40*, 191-197. 10.2144/000112096.
737 67. Kawaguchi, Y., Van Sant, C., and Roizman, B. (1997). Herpes simplex virus 1 alpha
738 regulatory protein ICP0 interacts with and stabilizes the cell cycle regulator cyclin
739 D3. J Virol *71*, 7328-7336. 10.1128/JVI.71.10.7328-7336.1997.
740 68. Sagou, K., Imai, T., Sagara, H., Uema, M., and Kawaguchi, Y. (2009). Regulation of
741 the catalytic activity of herpes simplex virus 1 protein kinase Us3 by
742 autophosphorylation and its role in pathogenesis. J Virol *83*, 5773-5783.
743 10.1128/JVI.00103-09.
744 69. Ritz, C. (2010). Toward a unified approach to dose-response modeling in ecotoxicology.
745 Environmental Toxicology and Chemistry *29*, 220-229. 10.1002/etc.7.
746 70. Ritz, C., Baty, F., Streibig, J.C., and Gerhard, D. (2015). Dose-Response Analysis
747 Using R. PLOS ONE *10*, e0146021. 10.1371/journal.pone.0146021.
748
749

ACKNOWLEDGEMENTS

We thank Risa Abe, Tohru Ikegami and Yui Muto for their excellent technical assistance. We acknowledge the NGS core facility of the Genome Information Research Center at the Research Institute for Microbial Diseases of Osaka University for the support in RNA sequencing and data analysis.

Funding: This study was supported by Grants for Scientific Research and Grant-in-Aid for Scientific Research (S) (20H05692) from the Japan Society for the Promotion of Science (JSPS), grants for Scientific Research on Innovative Areas (21H00338, 21H00417, 22H04803) and a grant for Transformative Research Areas (22H05584) from the Ministry of Education, Culture, Science, Sports and Technology of Japan, PRESTO (JPMJPR22R5), SPRING (JPMJSP2018), MIRAI (JPMJMI22G1) and Moonshot R&D (JPMJM2021, JPMJMS2025) from Japan Science and Technology Agency (JST), grants (JP20wm0125002, JP22fk0108640, JP22gm1610008, JP223fa627001, JP23wm0225031, JP23wm0225035) from the Japan Agency for Medical Research and Development (AMED), grants from the International Joint Research Project of the Institute of Medical Science, the University of Tokyo, and grants from the Takeda Science Foundation, the Uehara Memorial Foundation and the Mitsubishi Foundation.

767 **Author contributions:** Conceptualization: MN, YM, YK; Methodology: MN, YM, YK;
768 Investigation: MN, YM, KT, FM, HK, TN, SA; Resources: MN, YM, KT, NK, AK;
769 Formal analysis: MN, YM, RY, TN, HP, YK, SI; Visualization: MN, YM, RY, TN, HP,
770 YK, SI; Funding acquisition: YM, SI, AK, YK; Writing – original draft: MN, YM, YK;
771 Supervision: YK

772 **Competing interests:** The authors declare that they have no competing interests.

773 **Data and materials availability:** All data needed to evaluate the conclusions in the paper
774 are present in the paper and/or the Supplementary Materials. The mass spectrometry data
775 were deposited in the Japan ProteOme STandard Repository (jPOST) under the ID
776 JPST002328. RNA-seq data have been deposited to Gene Expression Omnibus (GEO)
777 with accession number GSE240449.
778

779 **FIGURE LEGENDS**

780 **Fig. 1. Characterization of the reporter HSV-1 rICP47/vUs11 generated in this study.**
781 (A) Schematic diagram of the genome structure of wild-type HSV-1(F) and
782 rICP47/vUs11. Line 1, wild-type HSV-1(F) genome; line 2, domains of the Us11 and
783 ICP47 coding regions. The positions of insertion of TagRFP and Venus are indicated. (B)
784 HeLa cells mock-infected or infected for 24 h with wild-type HSV-1(F) or rICP47/vUs11
785 at an MOI of 5 were lysed and analyzed by immunoblotting with the indicated antibodies.
786 (C) HeLa cells were infected at an MOI of 5 with wild-type HSV-1(F) or rICP47/vUs11.
787 Each cell culture supernatant plus the infected cells were harvested at the indicated times
788 post infection, and progeny viruses were assayed on Vero cells. (D) HeLa cells infected
789 for 24 h with wild-type HSV-1(F) or rICP47/vUs11 at an MOI of 5 were analyzed by
790 flow cytometry. (E) Quantitative bar graph of the proportion of cells in the
791 TagRFP/Venus (+/+), TagRFP/Venus (+/-), TagRFP/Venus (-/+), and TagRFP/Venus (-
792 /-) subpopulations shown in (D). (F) CV values for TagRFP-ICP47 and Venus-Us11
793 shown in (D). The data are representative of three independent experiments (B and D).
794 Each value is the mean ± standard error of the results of four (C) or three (E and F)
795 independent experiments. Statistical analysis was performed by unpaired Student's *t*-test.
796 ns, not significant (C and F).

797

798 **Fig. 2. Abundance of HSV-1 L proteins in each subpopulation of rICP47/vUs11-**
799 **infected cells.** (A) HeLa cells were infected for 24 h with rICP47/vUs11 at an MOI of 5
800 and sorted into six subpopulations (f1 to f6) by cell sorting as shown in S-Fig. 1A and

801 each subpopulation was analyzed by LC-MS/MS. The heatmap of $\log_{10}$ (relative
802 abundance) of 48 HSV-1 L proteins in each subpopulation is shown. Data are the mean
803 values from two biologically independent experiments. (B) Heatmap of the Pearson
804 correlation coefficient between $\log_{10}$ (MFI of Venus) of each subpopulation and $\log_{10}$
805 (relative abundance) of each HSV-1 L protein. P-values for the correlation coefficient of
806 all HSV-1 L proteins except Us8.5 shown in (B) were < 0.05.
807
808 **Fig. 3. Quantitative analysis of a relationship between the expression levels of HSV-**
809 **1 L proteins and progeny virus yields.** (A to G) HeLa cells were infected with
810 rICP47/vUs11 at an MOI of 5 and sorted as shown in S-Fig. 2. Sorted cells were sonicated
811 and virus titers were determined by plaque assay using Vero cells. (A) Kinetics of mean
812 fluorescent intensity (MFI) of Venus and progeny virus titers of the entire population. (B)
813 Scatter plot of $\log_{10}$(relative MFI of Venus) vs $\log_{10}$(PFU/10^4 cells) from panel A. (C)
814 Kinetics of progeny virus titers of the entire population from panel A (actual) and sum of
815 the virus titers produced by f1 to f6 subpopulation (virtual_f1-f6). The calculation method
816 for virtual titers is described in the Materials and methods. (D) Proportion of cells in the
817 indicated subpopulation account for the entire cell population at the indicated times after
818 infection. (E) Proportion of virus titers produced by the f1 to f6 subpopulations account
819 for virus titers produced by the entire population at the indicated times after infection. (F)
820 Scatter plots of $\log_{10}$(relative MFI of Venus) vs $\log_{10}$(PFU/10^4 cells). (G) Scatter plots of
821 $\log_{10}$(relative MFI of Venus) vs $\log_{10}$(PFU/10^4 cells) of the indicated subpopulations
822 separated by time after infection from panel F. Each value is the mean ± standard error

823 (A, C, D, E, F, and G) or individual value (B) of the results of three independent
824 experiments. Statistical analysis was performed by unpaired Student's *t*-test. ns, not
825 significant (C). Solid and dashed lines indicate 1 PFU/cell and 0.1 PFU/cell, respectively
826 (F and G).
827
828 **Fig. 4. Cells expressing higher than specific levels of HSV-1 L proteins have a**
829 **predominant role in yielding progeny infectious viruses.** (A) Kinetics of the sum of
830 the virus titers produced by f1 to f6 (virtual_f1-f6) or f4 to f6 (virtual_f4-f6)
831 subpopulations. (B) Kinetics of progeny virus titers of the entire population (actual) and
832 sum of the virus titers produced by f4 to f6 subpopulations (virtual_f4-f6). (C) Scatter
833 plot of $\log_{10}$(relative MFI of Venus) vs $\log_{10}$(PFU/10^4 cells) of subpopulations. (D)
834 Progeny virus titers of the f4 to f6 subpopulations at the indicated times after infection.
835 Each value is the mean ± standard error (A, B and D) or individual value (C) of the results
836 of three independent experiments. Statistical analysis was performed by unpaired
837 Student's *t*-test. ns, not significant. All data are obtained from the experiment shown in
838 Fig. 3.
839
840 **Fig. 5. Electron microscopic analysis of cells in the f2 to f5 subpopulations.** (A and
841 B) HeLa cells were infected with rICP47/vUs11 at an MOI of 5 and sorted into four
842 subpopulations (f2 to f5) by cell sorting 24 h after infection. Sorted cells were fixed,
843 embedded, sectioned, stained, and examined by electron microscopy. (A) A transmission
844 electron microscopy image of cells in the f2 to f5 subpopulations. n, nucleus; c, cytoplasm.

845 Scale bars = 500 nm. (B) The numbers of nuclear virions, enveloped virions in the
846 perinuclear space, naked capsids in the cytoplasm, and enveloped virions in the cytoplasm
847 of 11 cells in the f2 to f5 subpopulations were quantitated. The horizontal bars indicate
848 the means. Virions are marked in yellow.
849
850 **Fig. 6. Frequencies of A, B, and C capsids in the nucleus of cells in the f2 to f5**
851 **subpopulations.** (A) The numbers of A, B, and C capsids in the nucleus of 11 cells
852 analyzed in Fig. 4 in the f2 to f5 subpopulations were quantitated. The horizontal bars
853 indicate the means. Proportions of A, B, and C capsids to nuclear capsids (B), or virions
854 in the perinuclear space and cytoplasm (C) of cells with more than two nuclear capsids
855 (f3, n = 9; f4, n = 11; f5, n = 11). Data are presented as the median ± interquartile range
856 (IQR). Statistical analysis was performed by the Mann-Whitney *U*-test, and P-values
857 were adjusted by Bonferroni correction. ns, not significant.
858
859 **Fig. 7. Unique protein expression profiles of a subset of HSV-1 L proteins.** (A) Scatter
860 plots of $\log_{10}$(relative MFI of Venus) vs $\log_{10}$(relative abundance) of L proteins (from S-
861 Fig. 1B) of the bottom 10 HSV-1 L proteins with relatively low correlation coefficients
862 between fluorescence intensity of Venus and their abundance (from Fig. 2B). Plots of
863 terminase subunits are marked with magenta squares. (B) Threshold value (TV) of 48 L
864 proteins (from S-Fig. 10). (C) Scatter plots of $\log_{10}$(relative MFI of Venus) vs
865 $\log_{10}$(relative abundance) (from S-Fig. 1B) of the top 10 HSV-1 L proteins with highest
866 TV (from S-Fig. 10). Data of terminase subunits are shown in magenta.

867

868 **Supplementary Fig. 1. Abundance of HSV-1 L proteins in each subpopulation of**
869 **rICP47/vUs11 infected cells.** (A) Gating strategy for the LC-MS/MS analysis of HeLa
870 cells infected with rICP47/vUs11 at an MOI of 5 for 24 h. (B) Scatter plots of
871 $\log_{10}$(relative MFI of Venus) vs $\log_{10}$(relative abundances) of the 5 indicated HSV-1 IE
872 proteins, 13 indicated E proteins, and 48 indicated L proteins. Each value is the mean of
873 two biologically independent experiments. Individual value from two independent
874 experiments is plotted as a gray circle.

875

876 **Supplementary Fig. 2. Gating strategy for the experiments shown in Fig. 3.** HeLa
877 cells were infected with rICP47/vUs11 at an MOI of 5, analyzed by flow cytometry, and
878 sorted into an entire cell population (FSC singlet) or f1 to f6 subpopulations by cell sorting
879 at the indicated times after infection. Sorted cells were analyzed as shown in Fig 3.

880

881 **Supplementary Fig. 3. Quantitative analysis of the relationship between the**
882 **expression levels of HSV-1 L proteins and progeny virus yields at different MOIs.**
883 (A to G) HeLa cells infected with rICP47/vUs11 at the indicated MOI for 24 h, were
884 sorted into f1 to f6 subpopulations (A), sonicated and virus titers were determined by
885 plaque assay using Vero cells. (B) Scatter plot of $\log_{10}$(relative MFI of Venus) vs
886 $\log_{10}$(PFU/10^4 cells). (C) Proportion of cells in the indicated subpopulations account for
887 the entire cell population at the indicated MOIs. (D) Proportion of virus titers produced
888 by the f1 to f6 subpopulations account for virus titers produced by the entire population

889 at the indicated times after infection. (E to G) Progeny virus titers of the entire population
890 (actual) and sum of the virus titers produced by f1 to f6 (virtual_f1-f6) or f4 to f6
891 (virtual_f4-f6) subpopulations at the indicated MOIs. The data are representative of five
892 independent experiments (A). Each value is the mean ± standard error of the results of
893 five independent experiments (B to G). Statistical analysis was performed by one-way
894 ANOVA followed by the Tukey test (E to G). n.s., not significant
895
896 **Supplementary Fig. 4. Quantitative analysis of the relationship between the**
897 **expression levels of HSV-1 L proteins and progeny virus yields using different cell**
898 **lines.** Vero (A to E), U2OS (F to J), HaCaT (K to O), or HFFF-2 (P to T) cells infected
899 with rICP47/vUs11 at an MOI of 1 (A to E, and K to T) or 2.5 (F to J) for 12 h, were
900 sorted into f1 to f6 subpopulations (A, F, K, and P), sonicated, and virus titers were
901 determined by plaque assay using Vero cells. (B, G, L, and Q) Scatter plots of
902 $\log_{10}$(relative MFI of Venus) vs $\log_{10}$(PFU/10^4 cells) of each subpopulation. (C, H, M,
903 and R) Proportion of cells in the f1 to f6 subpopulations account for the entire cell
904 population. (D, I, N, and S) Proportion of virus titers produced by each subpopulation
905 account for the virus titers produced by the entire cell population. (E, J, O, and T) Progeny
906 virus titers of the entire population (actual) and sum of the virus titers produced by f1 to
907 f6 or f4 to f6 subpopulations. The data are representative of three (F) or four (A, K, and
908 P) independent experiments. Each value is the mean ± standard error of the results of
909 three (G to J) or four (B to E, L to O, and Q to T) independent experiments. Solid and
910 dashed lines indicate 1 PFU/cell and 0.1 PFU/cell, respectively (B, G, L and Q). Statistical

911 analysis was performed by one-way ANOVA followed by the Tukey test. n.s., not
912 significant (E, J, O, and T).
913
914 **Supplementary Fig. 5. Electron microscopic analysis of cells in the f2 to f4**
915 **subpopulations at 8 h after infection.** (A and B) HeLa cells were infected with
916 rICP47/vUs11 at an MOI of 5 and sorted into three subpopulations (f2 to f4) by cell
917 sorting 8 h after infection. Sorted cells were fixed, embedded, sectioned, stained, and
918 examined by electron microscopy. (A) A transmission electron microscopy image of cells
919 in the f2 to f4 subpopulations. n, nucleus; c, cytoplasm. Scale bar = 500 nm. (B) The
920 numbers of nuclear virions, enveloped virions in the perinuclear space, naked capsids in
921 the cytoplasm, and enveloped virions in the cytoplasm of 11 cells in the f2 to f4
922 subpopulations were quantitated. The horizontal bars indicate the means. Enveloped
923 virions and naked capsids are marked in yellow.
924
925 **Supplementary Fig. 6. f4 to f6 subpopulations have a predominant role in yielding**
926 **progeny infectious viruses.** (A) Scatter plots of $\log_{10}$(relative MFI of Venus) vs PFU/10^4
927 cells of the indicated subpopulation separated by time after infection from Fig. 3 panel G.
928 Scatter plots under the same conditions of electron microscopic analysis performed in Fig.
929 5 and S-Fig. 5 are shown in magenta. (B) Progeny virus titers of the f4 to f6
930 subpopulations at the indicated times after infection from Fig. 4 panel B. Statistical
931 analysis was performed by one-way ANOVA followed by the Tukey test. n.s., not
932 significant.

933

934 **Supplementary Fig. 7. Amount of HSV-1 DNA and mRNA in the f1 to f6**
935 **subpopulations.** (A and B) HeLa cells were infected for 24 h with rICP47/vUs11 at an
936 MOI of 5 and sorted into six subpopulations (f1 to f6) by cell sorting. Relative amounts
937 of HSV-1 DNA (A) and mRNA (B) of selected genes in each subpopulation were
938 analyzed by quantitative PCR or RNA-seq, respectively. Scatter plot of $\log_{10}$(relative MFI
939 of Venus) vs $\log_{10}$(relative amount of HSV-1 DNA) (A), or scatter plots of $\log_{10}$(relative
940 MFI of Venus) vs $\log_{10}$(relative FPKM) of the indicated HSV-1 genes (B) are shown.
941 Each value is the mean ± standard error of the results of three biologically independent
942 samples.

943

944 **Supplementary Fig. 8. Frequency of A, B, and C capsids in the nucleus of cells in f2**
945 **to f5 subpopulations.** A transmission electron microscopy image of cells in the f2 to f5
946 subpopulations. n, nucleus; c, cytoplasm from the experiment in Fig. 6. Type A capsids
947 are marked in green, B capsids in blue, and C capsids in red. Scale bars = 500 nm.

948

949 **Supplementary Fig. 9. Frequencies of B and C capsids in the nucleus of cells in the**
950 **f2 to f4 subpopulations at 8 h after infection.** (A) A transmission electron microscopy
951 image of cells in the f2 to f4 subpopulations. n, nucleus; c, cytoplasm from the experiment
952 in S-Fig. 6. Type A capsids are marked in green, B capsids in blue, and C capsids in red.
953 Scale bar = 500 nm. (B) The numbers of A, B, and C capsids in the nucleus of 11 cells
954 analyzed in S-Fig. 6 in the f2 to f4 subpopulations were quantitated. The horizontal bars

955 indicate the means. Proportions of B and C capsids to nuclear capsids (C), or virions in
956 the perinuclear space and cytoplasm (D) of cells with more than two nuclear capsids (f3,
957 n = 11; f4, n = 11). Data are presented as the median ± interquartile range (IQR).
958 Statistical analysis was performed by the Mann-Whitney *U*-test.
959
960 **Supplementary Fig. 10. Curve fitting to abundance profiles of HSV-1 L proteins.**
961 Scatter plots of $\log_{10}$(relative MFI of Venus) vs $\log_{10}$(relative abundances) of the 48
962 indicated HSV-1 L proteins (from S-Fig. 1B) were fitted to a four-parameter logistic
963 regression curve. TVs are the x-axis value at which the y-axis value increases by $\log_{10}2$
964 (2-fold increase in linear scale) from the starting point (x = 0) for each curve. The grey
965 regions correspond to 95% confidence intervals. The average value of two biologically
966 independent experiments was used for curve fitting.

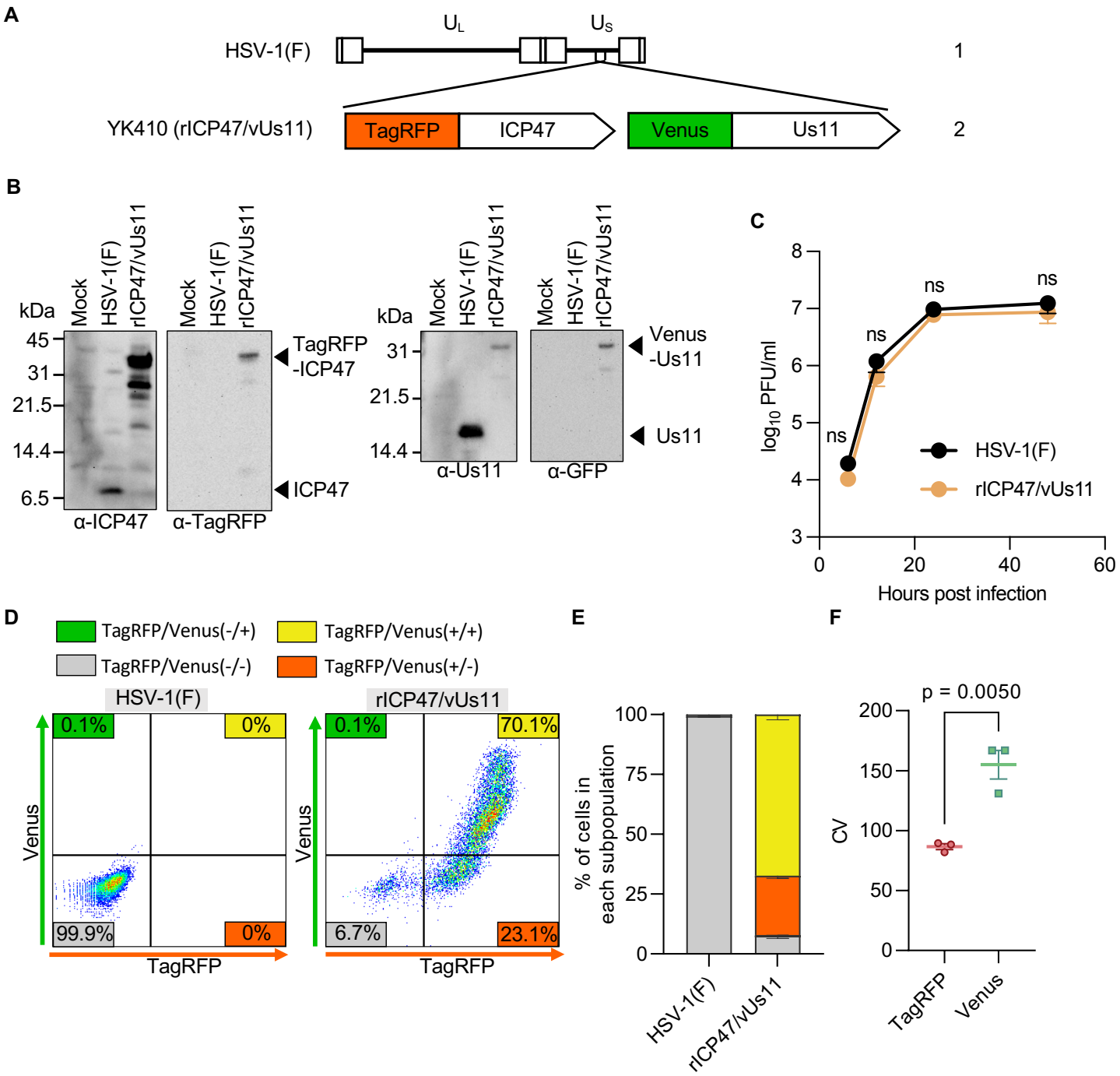

Fig. 1. Characterization of the reporter HSV-1 rICP47/vUs11 generated in this study. (A) Schematic diagram of the genome structure of wild-type HSV-1(F) and rICP47/vUs11. Line 1, wild-type HSV-1(F) genome; line 2, domains of the Us11 and ICP47 coding regions. The positions of insertion of TagRFP and Venus are indicated. (B) HeLa cells mock-infected or infected for 24 h with wild-type HSV-1(F) or rICP47/vUs11 at an MOI of 5 were lysed and analyzed by immunoblotting with the indicated antibodies. (C) HeLa cells were infected at an MOI of 5 with wild-type HSV-1(F) or rICP47/vUs11. Each cell culture supernatant plus the infected cells were harvested at the indicated times post infection, and progeny viruses were assayed on Vero cells. (D) HeLa cells infected for 24 h with wild-type HSV-1(F) or rICP47/vUs11 at an MOI of 5 were analyzed by flow cytometry. (E) Quantitative bar graph of the proportion of cells in the TagRFP/Venus (+/+), TagRFP/Venus (+/-), TagRFP/Venus (-/+), and TagRFP/Venus (-/-) subpopulations shown in (D). (F) CV values for TagRFP-ICP47 and Venus-Us11 shown in (D). The data are representative of three independent experiments (B and D). Each value is the mean ± standard error of the results of four (C) or three (E and F) independent experiments. Statistical analysis was performed by unpaired Student's *t*-test. ns, not significant (C and F).

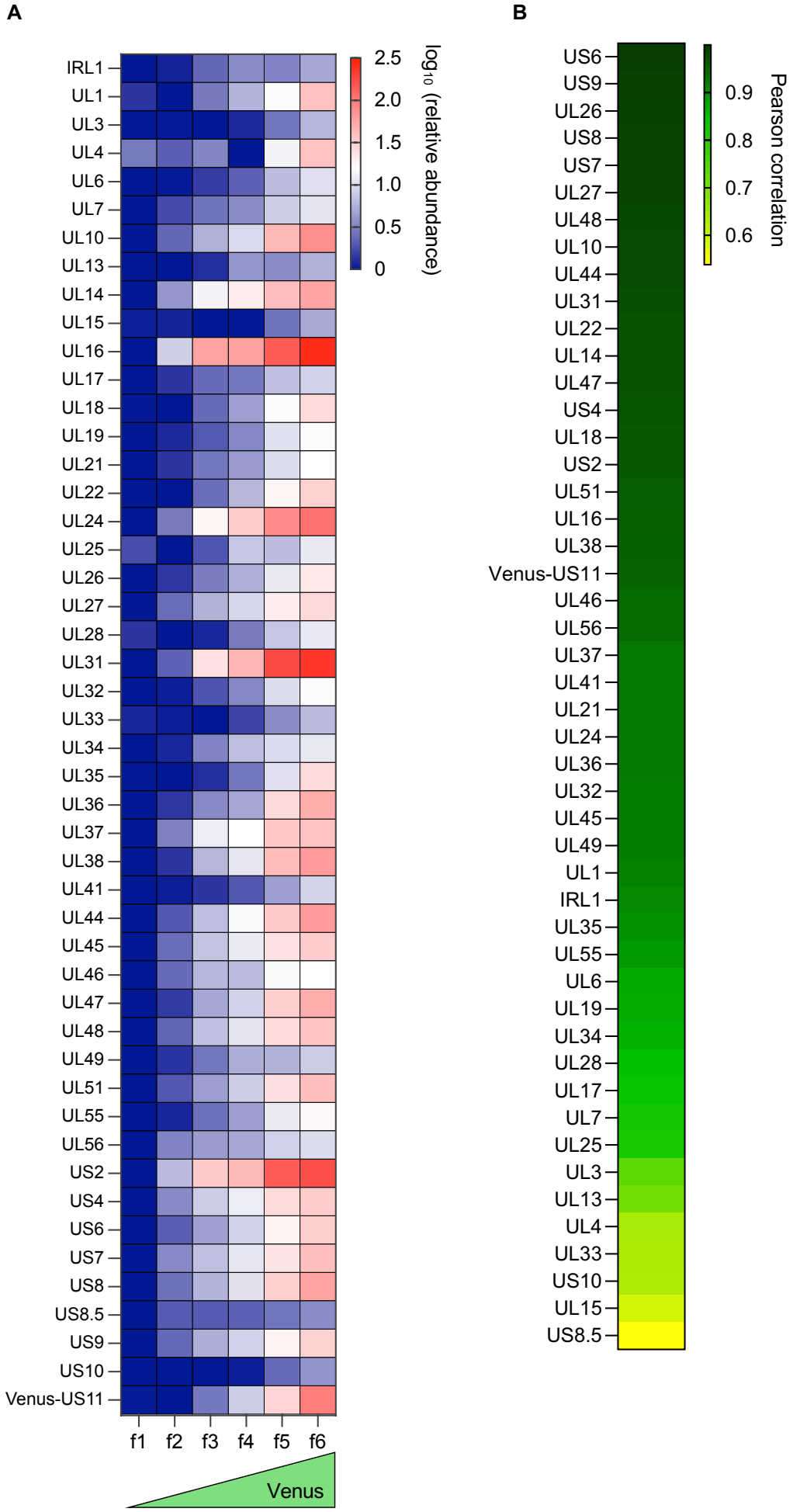

(Legend on next page)

Fig. 2 M. Nobe and Y. Maruzuru et al.

Fig. 2. Abundance of HSV-1 L proteins in each subpopulation of rICP47/vUs11-infected cells. (A) HeLa cells were infected for 24 h with rICP47/vUs11 at an MOI of 5 and sorted into six subpopulations (f1 to f6) by cell sorting as shown in S-Fig. 1A and each subpopulation was analyzed by LC-MS/MS. The heatmap of log10 (relative abundance) of 48 HSV-1 L proteins in each subpopulation is shown. Data are the mean values from two biologically independent experiments. (B) Heatmap of the Pearson correlation coefficient between $\log_{10}$ (MFI of Venus) of each subpopulation and $\log_{10}$ (relative abundance) of each HSV-1 L protein. P-values for the correlation coefficient of all HSV-1 L proteins except Us8.5 shown in (B) were < 0.05.

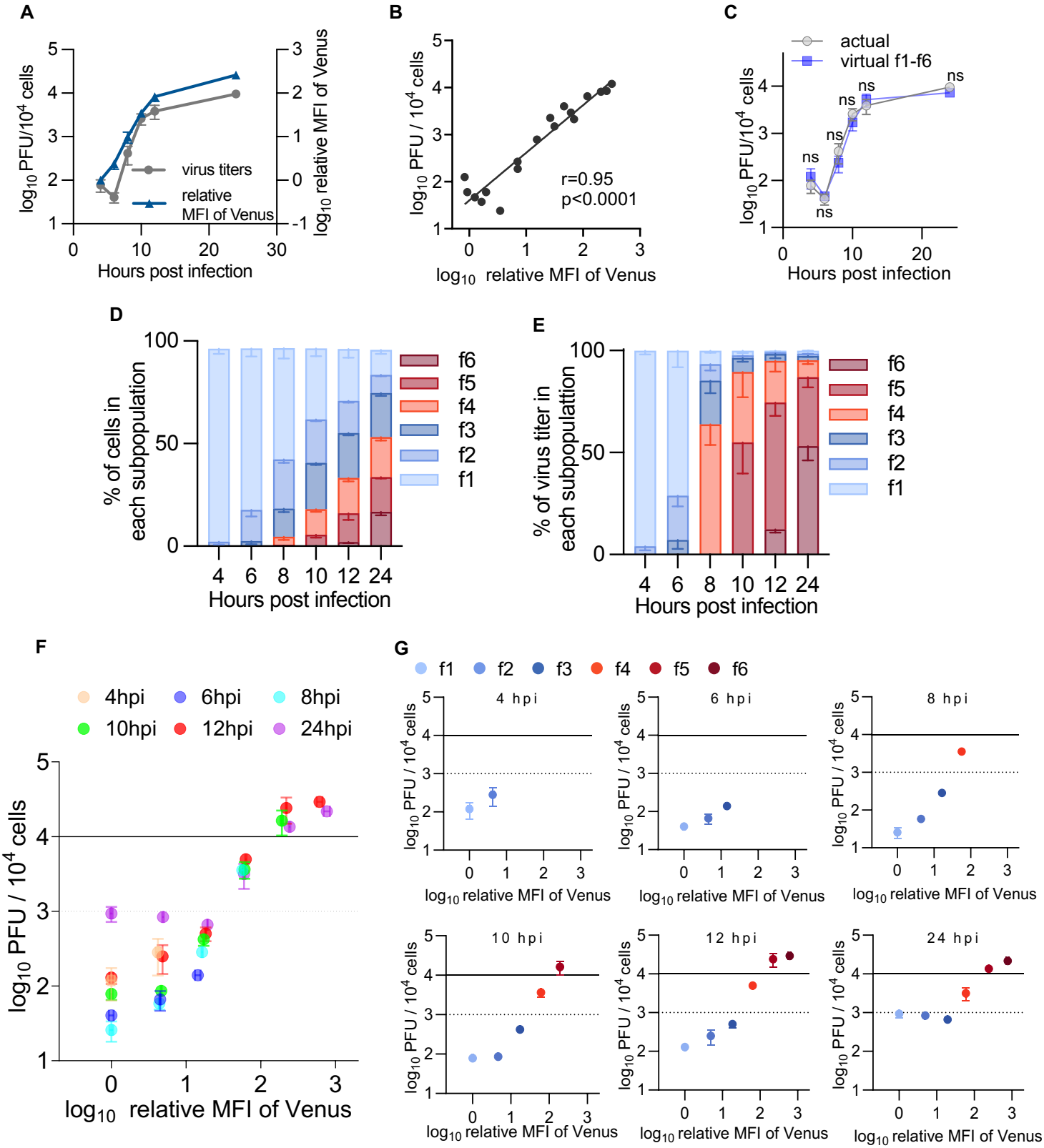

Fig. 3. Quantitative analysis of a relationship between the expression levels of HSV-1 L proteins and progeny virus yields. (A to G) HeLa cells were infected with rICP47/vUs11 at an MOI of 5 and sorted as shown in S-Fig. 2. Sorted cells were sonicated and virus titers were determined by plaque assay using Vero cells. (A) Kinetics of mean fluorescent intensity (MFI) of Venus and progeny virus titers of the entire population. (B) Scatter plot of $\log_{10}$(relative MFI of Venus) vs $\log_{10}$(PFU/10^4 cells) from panel A. (C) Kinetics of progeny virus titers of the entire population from panel A (actual) and sum of the virus titers produced by f1 to f6 subpopulation (virtual_f1-f6). The calculation method for virtual titers is described in the Materials and methods. (D) Proportion of cells in the indicated subpopulation account for the entire cell population at the indicated times after infection. (E) Proportion of virus titers produced by the f1 to f6 subpopulations account for virus titers produced by the entire population at the indicated times after infection. (F) Scatter plots of $\log_{10}$(relative MFI of Venus) vs $\log_{10}$(PFU/10^4 cells). (G) Scatter plots of $\log_{10}$(relative MFI of Venus) vs $\log_{10}$(PFU/10^4 cells) of the indicated subpopulations separated by time after infection from panel F. Each value is the mean ± standard error (A, C, D, E, F, and G) or individual value (B) of the results of three independent experiments. Statistical analysis was performed by unpaired Student's *t*-test. ns, not significant (C). Solid and dashed lines indicate 1 PFU/cell and 0.1 PFU/cell, respectively (F and G).

Fig. 3 M. Nobe and Y. Maruzuru et al.

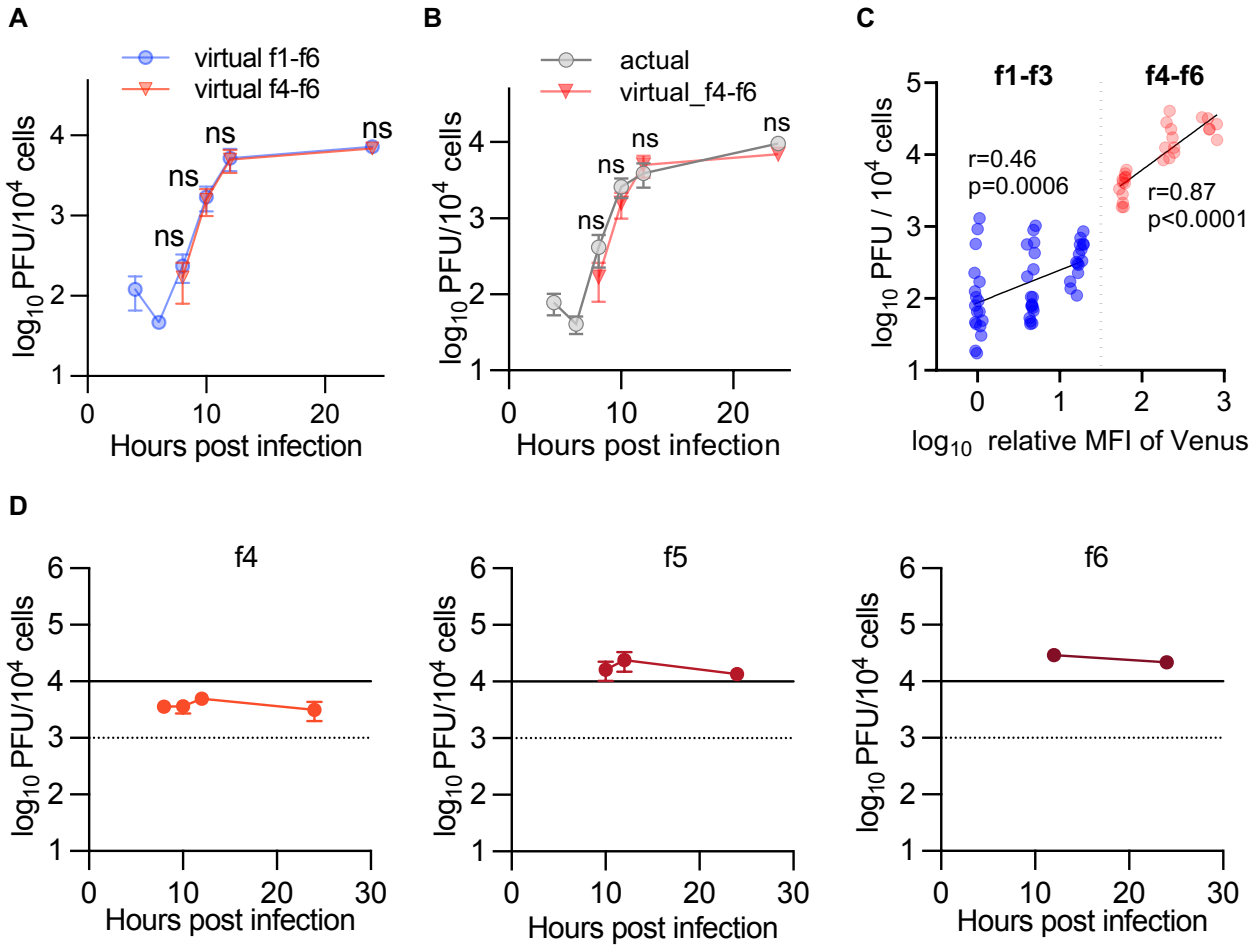

Fig. 4. Cells expressing higher than specific levels of HSV-1 L proteins have a predominant role in yielding progeny infectious viruses. (A) Kinetics of the sum of the virus titers produced by f1 to f6 (virtual_f1-f6) or f4 to f6 (virtual_f4-f6) subpopulations. (B) Kinetics of progeny virus titers of the entire population (actual) and sum of the virus titers produced by f4 to f6 subpopulations (virtual_f4-f6). (C) Scatter plot of $\log_{10}$(relative MFI of Venus) vs $\log_{10}$(PFU/10^4 cells) of subpopulations. (D) Progeny virus titers of the f4 to f6 subpopulations at the indicated times after infection. Each value is the mean ± standard error (A, B and D) or individual value (C) of the results of three independent experiments. Statistical analysis was performed by unpaired Student's *t*-test. ns, not significant. All data are obtained from the experiment shown in Fig. 3.

A

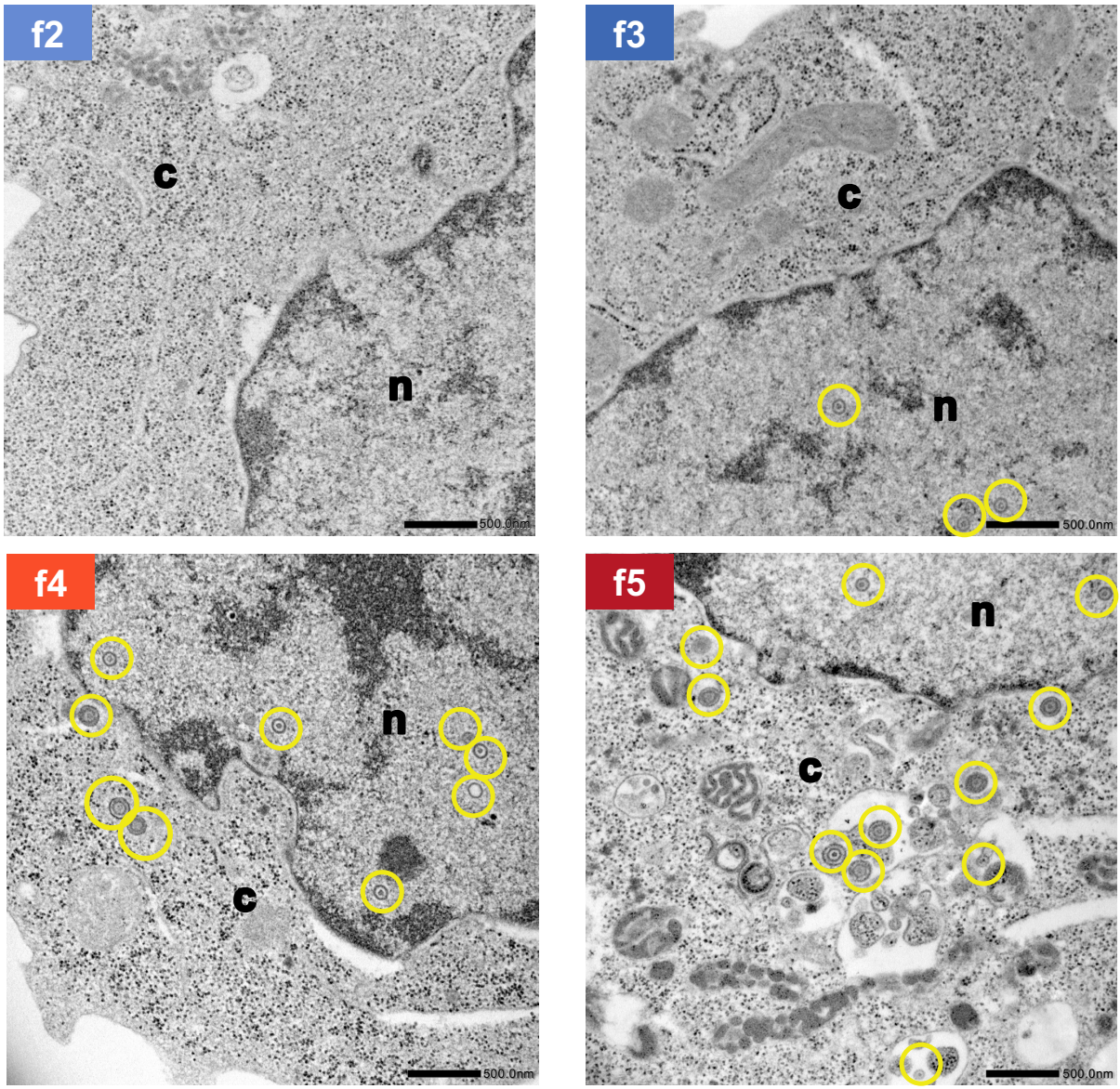

B

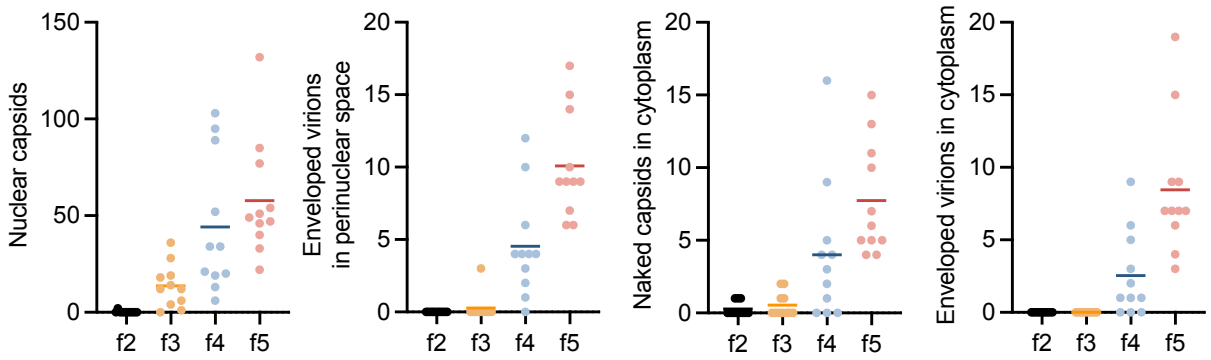

Fig. 5. Electron microscopic analysis of cells in the f2 to f5 subpopulations. (A and B) HeLa cells were infected with rICP47/vUs11 at an MOI of 5 and sorted into four subpopulations (f2 to f5) by cell sorting 24 h after infection. Sorted cells were fixed, embedded, sectioned, stained, and examined by electron microscopy. (A) A transmission electron microscopy image of cells in the f2 to f5 subpopulations. n, nucleus; c, cytoplasm. Scale bars = 500 nm. (B) The numbers of nuclear virions, enveloped virions in the perinuclear space, naked capsids in the cytoplasm, and enveloped virions in the cytoplasm of 11 cells in the f2 to f5 subpopulations were quantitated. The horizontal bars indicate the means. Virions are marked in yellow.

Fig. 5 M. Nobe and Y. Maruzuru et al.

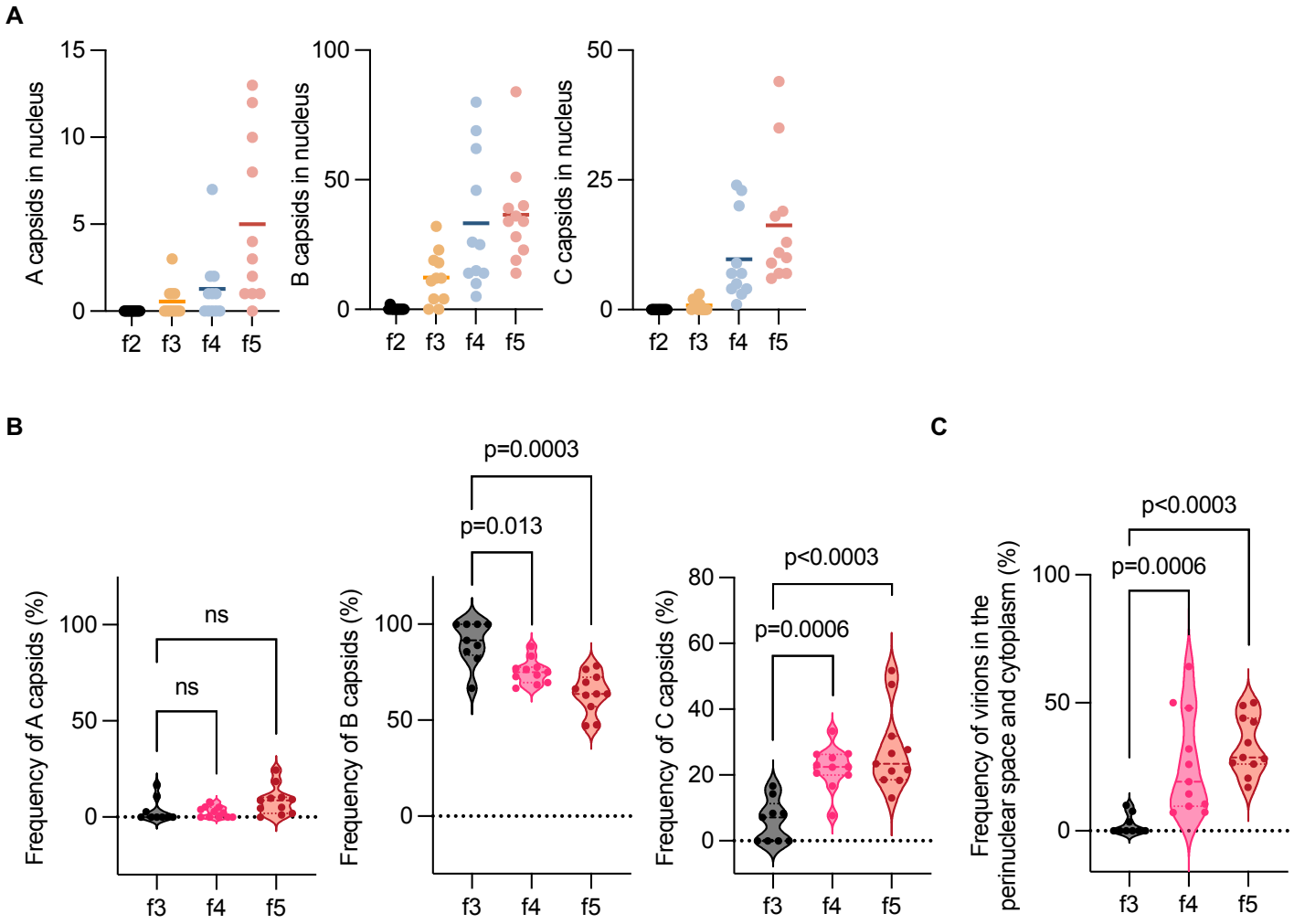

Fig. 6. Frequencies of A, B, and C capsids in the nucleus of cells in the f2 to f5 subpopulations. (A) The numbers of A, B, and C capsids in the nucleus of 11 cells analyzed in Fig. 4 in the f2 to f5 subpopulations were quantitated. The horizontal bars indicate the means. Proportions of A, B, and C capsids to nuclear capsids (B), or virions in the perinuclear space and cytoplasm (C) of cells with more than two nuclear capsids (f3, n = 9; f4, n = 11; f5, n = 11). Data are presented as the median ± interquartile range (IQR). Statistical analysis was performed by the Mann-Whitney *U*-test, and P-values were adjusted by Bonferroni correction. ns, not significant.

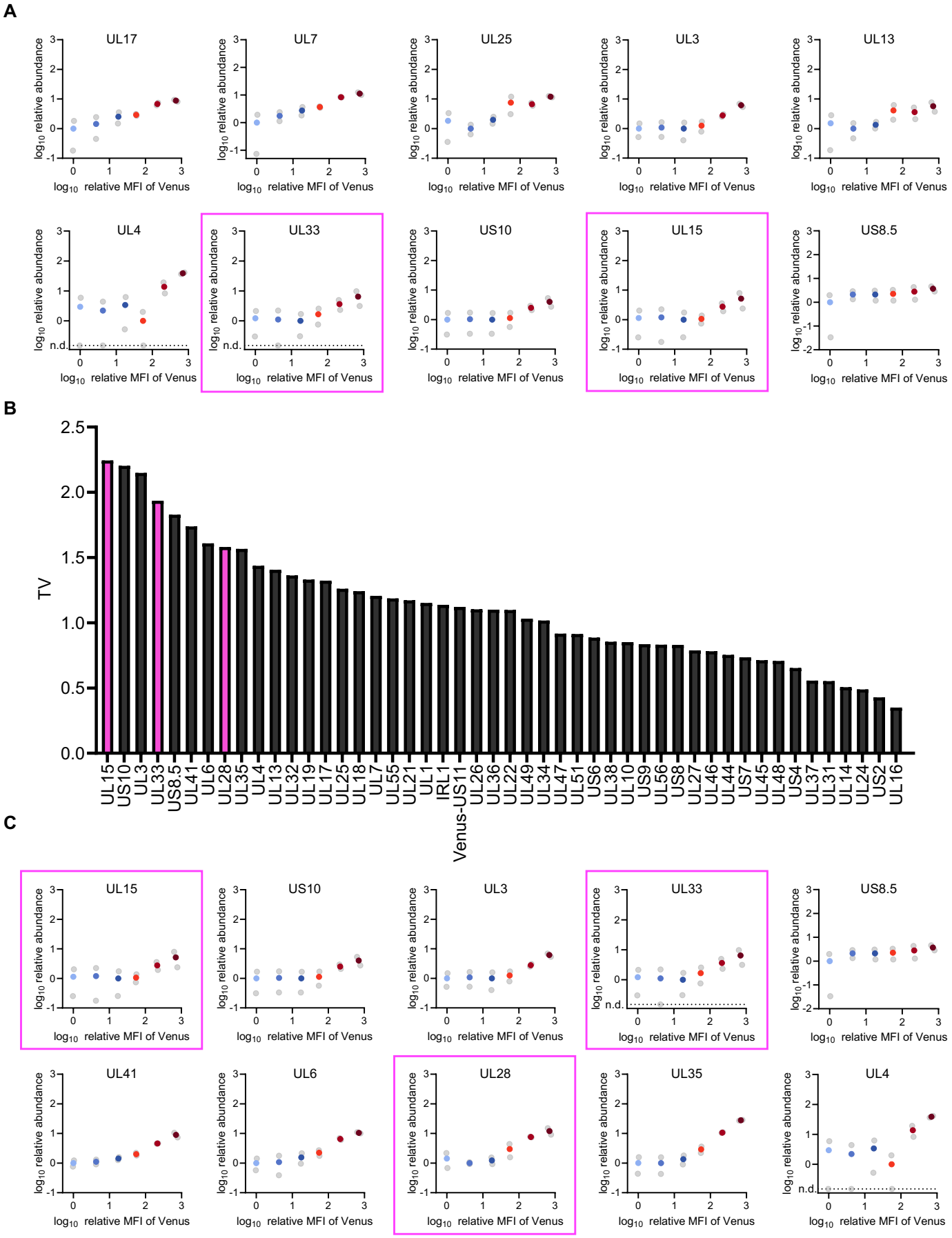

Fig. 7. Unique protein expression profiles of a subset of HSV-1 L proteins. (A) Scatter plots of $\log_{10}$(relative MFI of Venus) vs $\log_{10}$(relative abundance) of L proteins (from S-Fig. 1B) of the bottom 10 HSV-1 L proteins with relatively low correlation coefficients between fluorescence intensity of Venus and their abundance (from Fig. 2B). Plots of terminase subunits are marked with magenta squares. (B) Threshold value (TV) of 48 L proteins (from S-Fig. 10). (C) Scatter plots of $\log_{10}$(relative MFI of Venus) vs $\log_{10}$(relative abundance) (from S-Fig. 1B) of the top 10 HSV-1 L proteins with highest TV (from S-Fig. 10). Data of terminase subunits are shown in magenta.